

# Conical Horn Antenna

A theoretical approach

Tworit Kumar Dash



# Conical Horn Antenna

## A theoretical approach

by

Tworit Kumar Dash

to obtain the degree of Master of Science  
at the Delft University of Technology,

Student number: 4816315  
Project duration: November 11, 2019 – July 3, 2020  
Thesis committee: Prof. DSc. A. Yarovoy, TU Delft, supervisor  
dr. D. Prinsloo, ASTRON

An electronic version of this thesis is available at <http://repository.tudelft.nl/>.





# Preface

Preface...

*Tworit Kumar Dash  
Delft, January 2020*



# Contents

<b>1</b>	<b>Introduction</b>	<b>1</b>
<b>2</b>	<b>Circular Cross-Section Waveguides: Near Field Patterns</b>	<b>3</b>
2.1	$TE^z$ modes: . . . . .	3
2.2	$TM^z$ modes: . . . . .	6
2.3	Results: Near field or the field distribution on the aperture . . . . .	7
<b>3</b>	<b>Two Circular Cross-Section Waveguides with Mode Matching Technique</b>	<b>15</b>
3.1	Field Expressions for Circular Cross Section Waveguide . . . . .	15
3.1.1	Formulation of the Normalization Constant Q for each Mode and its Numerical solution . . . . .	16
3.1.2	An analytical approach for Solving for Normalization Constant Q . . . . .	17
3.1.3	Mode Matching Technique . . . . .	18
3.2	Formulation of the Inner Cross-Product X . . . . .	20
3.2.1	Formulation of Inner Cross Product using Normalized Field Equations . . . . .	21
3.2.2	Analytical Formulation of the Inner Cross Product for modes TE, TE and TM, TM combination . . . . .	24
3.3	Convergence of Mode Matching Technique . . . . .	24
3.3.1	Feko Simulations and Comparison . . . . .	26
<b>4</b>	<b>Cascaded Circular Cross-Section Waveguides with Mode Matching Technique</b>	<b>31</b>
4.1	Formulation of GSM . . . . .	31
4.1.1	Convergence with 3 waveguide structure . . . . .	33
4.1.2	Feko simulation and comparison . . . . .	34
	<b>Bibliography</b>	<b>37</b>



# 1

## Introduction



# 2

## Circular Cross-Section Waveguides: Near Field Patterns

To understand the behaviour of a conical horn antenna, a single circular cross-section waveguide needs to be studied. Later, multiple circular cross-section waveguides were analysed by placing them one after the other to resemble a cone structure waveguide horn. In this section, a circular waveguide is studied based on text-book approach [1]. The waveguide modes, those are supported by these waveguide configurations are  $TE^z$  and  $TM^z$ . Here z axis is the direction of propagation of the wave.

### 2.1. $TE^z$ modes:

The TE modes can be derived from the vector potentials A (Electric field potential) and F (Magnetic field potential).

$$A = 0 \quad (2.1)$$

$$F = \hat{z}F_z(\rho, \phi, z) \quad (2.2)$$

A cylindrical coordinate system is preferred in this case because of the ease of analysis of a cylindrical domain. The vector potential F should satisfy the following Helmholtz equation:

$$\nabla^2 F_z((\rho, \phi, z)) + \beta^2 F_z(\rho, \phi, z) = 0 \quad (2.3)$$

This reduces down to:

$$\frac{\partial^2 F_z}{\partial \rho^2} + \frac{1}{\rho} \frac{\partial F_z}{\partial \rho} + \frac{1}{\rho^2} \frac{\partial^2 F_z}{\partial \phi^2} + \frac{\partial^2 F_z}{\partial z^2} = -\beta^2 F_z \quad (2.4)$$

If we assume a solution with 3 independent functions of  $\rho$ ,  $\phi$  and  $z$ , we have:

$$F_z(\rho, \phi, z) = f(\rho)g(\phi)h(z) \quad (2.5)$$

Using this on equation 2.4, we have:

$$gh \frac{\partial^2 f}{\partial \rho^2} + gh \frac{1}{\rho} \frac{\partial f}{\partial \rho} + fh \frac{1}{\rho^2} \frac{\partial^2 g}{\partial \phi^2} + fg \frac{\partial^2 h}{\partial z^2} = -\beta^2 fgh \quad (2.6)$$

Dividing both sides by  $fgh$ , we have:

$$\frac{1}{f} \frac{\partial^2 f}{\partial \rho^2} + \frac{1}{\rho} \frac{\partial f}{\partial \rho} + \frac{1}{\rho^2} \frac{1}{g} \frac{\partial^2 g}{\partial \phi^2} + \frac{1}{h} \frac{\partial^2 h}{\partial z^2} = -\beta^2 \quad (2.7)$$

As the z dependence is only on the phase as it is a travelling wave along z, we can write:

$$\frac{\partial^2 h}{\partial z^2} = -\beta_z^2 h \quad (2.8)$$

Where,  $\beta_z$  is the wavenumber along the z direction.

Substituting this on equation 2.7 and multiplying  $\rho^2$  we have:

$$\frac{\rho^2}{f} \frac{\partial^2 f}{\partial \rho^2} + \frac{\rho}{f} \frac{\partial f}{\partial \rho} + \frac{1}{g} \frac{\partial^2 g}{\partial \phi^2} + \rho^2 (\beta^2 - \beta_z^2) = 0 \quad (2.9)$$

We can replace the term  $\frac{1}{g} \frac{\partial^2 g}{\partial \phi^2}$  as a constant as g only depends on  $\phi$ , therefore,

$$\frac{1}{g} \frac{\partial^2 g}{\partial \phi^2} = -m^2 \quad (2.10)$$

$\Rightarrow$

$$\frac{\partial^2 g}{\partial \phi^2} = -m^2 g \quad (2.11)$$

As we know that the wavenumber's  $\rho$  component can be found as  $\beta_\rho^2 = \beta^2 - \beta_z^2$ , we can reduce the equation 2.9 as follows:

$$\rho^2 \frac{\partial^2 f}{\partial \rho^2} + \rho \frac{\partial f}{\partial \rho} + [(\beta_\rho \rho) - m^2] f = 0 \quad (2.12)$$

This resembles Bessel's differential equation. The solutions are of the form:

$$F_z(\rho, \phi, z) = f(\rho)g(\phi)h(z) = [A_1 J_m(\beta_\rho \rho) + B_1 Y_m(\beta_\rho \rho)][C_2 \cos(m\phi) + D_2 \sin(m\phi)][A_3 e^{-j\beta_z z} + B_3 e^{j\beta_z z}] \quad (2.13)$$

These solutions for f, g and h were chosen because for this cylindrical waveguide it is more practical to think of standing waves along the  $\phi$  direction, standing waves along the  $\rho$  direction and travelling waves on the z direction. Here  $J_m$  and  $Y_m$  are the Bessel functions of first and second kind.

To find out the constants, we can use the boundary conditions:

The boundary conditions (BCs) are:

- $E_\phi(\rho = a, \phi, z) = 0$
- The fields must be finite everywhere
- The field must repeat after  $2\pi$  radians in  $\phi$ .

Following the second BC, we have  $B_1 = 0$  as  $Y_m(\rho = 0) = \infty$ . According to the third BC of periodicity over  $\phi$ , we can conclude that  $m = 0, 1, 2, 3, \dots$ . If we consider no reflection from the other boundary of the waveguide ( $B_3 = 0$ ), we can rewrite the equation 2.13 as:

$$F_z(\rho, \phi, z) = A_{mn} J_m(\beta_\rho \rho) [C_2 \cos(m\phi) + D_2 \sin(m\phi)] e^{-j\beta_z z} \quad (2.14)$$

Therefore, for this completely matched (No reflection) waveguide, the  $\phi$  component of the electric field is:

$$E_\phi(\rho, \phi, z) = \frac{1}{\epsilon} \frac{\partial F_z}{\partial \rho} = A_{mn} \frac{\beta_\rho}{\epsilon} J'_m(\beta_\rho \rho) [C_2 \cos(m\phi) + D_2 \sin(m\phi)] e^{-j\beta_z z} \quad (2.15)$$

Using the first BC, we have:

$$E_\phi(\rho = a, \phi, z) = A_{mn} \frac{\beta_\rho}{\epsilon} J'_m(\beta_\rho a) [C_2 \cos(m\phi) + D_2 \sin(m\phi)] e^{-j\beta_z z} \quad (2.16)$$

This can only be true if:

$$J'_m(\beta_\rho a) = 0 \quad (2.17)$$

$\Rightarrow$

$$\beta_\rho = \frac{\chi'_{mn}}{a} \quad (2.18)$$

Where,  $\chi'_{mn}$  is the nth zero of the derivative of the Bessel's function  $J_m$  of the first kind of the order m ( $0, 1, 2, 3, \dots$ ).

The  $\beta_z$  of the  $TE_{mn}$  mode can be written as:

$$(\beta_z)_{mn} = -j\sqrt{-(\beta^2 - \beta_\rho^2)} \quad (2.19)$$

This way of representing makes it easier to visualise that  $(\beta_z)_{mn}$  is purely real when  $\beta > \beta_\rho$ , purely imaginary when  $\beta < \beta_\rho$  and 0 when  $\beta = \beta_\rho$ . Therefore, cut off is determined by:

$$(\beta_z)_{mn} = 0 \quad (2.20)$$

$\Rightarrow$

$$\beta_c = \omega_c \sqrt{\mu \epsilon} = \beta_\rho \quad (2.21)$$

$\Rightarrow$

$$(f_c)_{mn} = \frac{\chi'_{mn}}{2\pi a \sqrt{\mu \epsilon}} \quad (2.22)$$

The electric field equations for a perfectly matched cylindrical waveguide are:

$$E_\rho = -\frac{1}{\epsilon \rho} \frac{\partial F_z}{\partial \phi} = -A_{mn} \frac{m}{\epsilon \rho} J_m(\beta_\rho \rho) [-C_2 \sin(m\phi) + D_2 \cos(m\phi)] e^{-j\beta_z z} \quad (2.23)$$

$$E_\phi = \frac{1}{\epsilon} \frac{\partial F_z}{\partial \rho} = A_{mn} \frac{\beta_\rho}{\epsilon} J'_m(\beta_\rho \rho) [C_2 \cos(m\phi) + D_2 \sin(m\phi)] e^{-j\beta_z z} \quad (2.24)$$

$$E_z = 0 \quad (2.25)$$

The magnetic field equations for a perfectly matched cylindrical waveguide are:

$$H_\rho = -j \frac{1}{\omega \mu \epsilon} \frac{\partial^2 F_z}{\partial \rho \partial z} = -A_{mn} \frac{\beta_\rho \beta_z}{\omega \mu \epsilon} J'_m(\beta_\rho \rho) [C_2 \cos(m\phi) + D_2 \sin(m\phi)] e^{-j\beta_z z} \quad (2.26)$$

$$H_\phi = -j \frac{1}{\omega \mu \epsilon} \frac{1}{\rho} \frac{\partial^2 F_z}{\partial \phi \partial z} = -A_{mn} \frac{m \beta_z}{\omega \mu \epsilon} \frac{1}{\rho} J_m(\beta_\rho \rho) [-C_2 \sin(m\phi) + D_2 \cos(m\phi)] e^{-j\beta_z z} \quad (2.27)$$

$$H_z = -j \frac{1}{\omega \mu \epsilon} \left( \frac{\partial^2}{\partial z^2} + \beta^2 \right) F_z = -j A_{mn} \frac{\beta_\rho^2}{\omega \mu \epsilon} J_m(\beta_\rho \rho) [C_2 \cos(m\phi) + D_2 \sin(m\phi)] e^{-j\beta_z z} \quad (2.28)$$

The impedance of the wave for TE modes, hence, can be determined as:

$$(Z_w)_{mn}^{TE} = \frac{E_\rho}{H_\phi} = \frac{-E_\phi}{H_\rho} = \frac{\omega \mu}{(\beta_z)_{mn}} \quad (2.29)$$

Therefore, Impedance of the wave is real above cut-off and imaginary below the cut off and inductive. Below cut off, it stores energy. Exactly at cut off the impedance is very high ( $\infty$ ).

## 2.2. $TM^z$ modes:

The same analysis can be done for the TM mode with the electric potential function.

$$F = 0 \quad (2.30)$$

$$A = \hat{z}A_z(\rho, \phi, z) \quad (2.31)$$

And the boundary conditions are:

- $E_\phi(\rho = a, \phi, z) = 0$
- $E_z(\rho = a, \phi, z) = 0$
- The fields must be finite everywhere
- The field must repeat after  $2\pi$  radians in  $\phi$ .

Using these, the solution to the PDE for a perfectly matched waveguide (No reflection) can be written as:

$$A_z(\rho, \phi, z) = B_{mn}J_m(\beta_\rho\rho)[C_2 \cos(m\phi) + D_2 \sin(m\phi)]e^{-j\beta_z z} \quad (2.32)$$

Using the second BC, it can be shown that,

$$J_m(\beta_\rho a) = 0 \quad (2.33)$$

$\Rightarrow$

$$\beta_\rho = \frac{\chi'_{mn}}{a} \quad (2.34)$$

Where,  $\chi'_{mn}$  is the nth zero of the Bessel's function  $J_m$  of the first kind of the order m (0, 1, 2, 3,...). Cut off frequency can be given as:

$$(f_c)_{mn} = \frac{\chi_{mn}}{2\pi a \sqrt{\mu\epsilon}} \quad (2.35)$$

The magnetic field equations for a perfectly matched cylindrical waveguide are:

$$H_\rho = \frac{1}{\mu\rho} \frac{\partial A_z}{\partial\phi} = B_{mn} \frac{m}{\mu\rho} J_m(\beta_\rho\rho)[-C_2 \sin(m\phi) + D_2 \cos(m\phi)]e^{-j\beta_z z} \quad (2.36)$$

$$H_\phi = \frac{1}{\mu} \frac{\partial A_z}{\partial\rho} = -B_{mn} \frac{\beta_\rho}{\mu} J'_m(\beta_\rho\rho)[C_2 \cos(m\phi) + D_2 \sin(m\phi)]e^{-j\beta_z z} \quad (2.37)$$

$$H_z = 0 \quad (2.38)$$

The electric field equations for a perfectly matched cylindrical waveguide are:

$$E_\rho = -j \frac{1}{\omega\mu\epsilon} \frac{\partial^2 A_z}{\partial\rho\partial z} = -B_{mn} \frac{\beta_\rho\beta_z}{\omega\mu\epsilon} J'_m(\beta_\rho\rho)[C_2 \cos(m\phi) + D_2 \sin(m\phi)]e^{-j\beta_z z} \quad (2.39)$$

$$E_\phi = -j \frac{1}{\omega\mu\epsilon} \frac{1}{\rho} \frac{\partial^2 A_z}{\partial\phi\partial z} = -B_{mn} \frac{m\beta_z}{\omega\mu\epsilon} \frac{1}{\rho} J_m(\beta_\rho\rho)[-C_2 \sin(m\phi) + D_2 \cos(m\phi)]e^{-j\beta_z z} \quad (2.40)$$

$$E_z = -j \frac{1}{\omega\mu\epsilon} \left( \frac{\partial^2}{\partial z^2} + \beta^2 \right) A_z = -j B_{mn} \frac{\beta_\rho^2}{\omega\mu\epsilon} J_m(\beta_\rho\rho)[C_2 \cos(m\phi) + D_2 \sin(m\phi)]e^{-j\beta_z z} \quad (2.41)$$

The impedance of the wave for TM modes, hence, can be determined as:

$$(Z_w)_{mn}^{TM} = \frac{E_\rho}{H_\phi} = \frac{-E_\phi}{H_\rho} = \frac{(\beta_z)_{mn}}{\omega\epsilon} \quad (2.42)$$

## 2.3. Results: Near field or the field distribution on the aperture

The above equations for near field pattern were plotted in MATLAB. For the plots. I have taken the constant  $C_2 = 1$  and  $D_2 = 0$ . The plot is at a particular cross-section ( $z = 0$ ).

The TE modes are shown in figure 2.1. For TE modes, the surface plot is the Electric field and the quiver plots (field lines) are for the magnetic field. The TM modes are shown in figure 2.2. For TM modes, the surface plots are magnetic field and the quiver plots (field lines) are for electric field.

In all these MATLAB simulations, the frequency was chosen to be a little bit higher than the cut off frequency of the respective modes.

Some results from Feko simulation are shown in figure 2.3. The patterns exactly match the analytical solution plotted in Matlab. The solver in Feko was Method of Moments (MoM). The source for this cylindrical structure was chosen to be a waveguide source which allows a certain mode. The cylinder is shown in figure 2.4. It is a cylinder of which one of the sides is open and the other side is excited by a waveguide source.

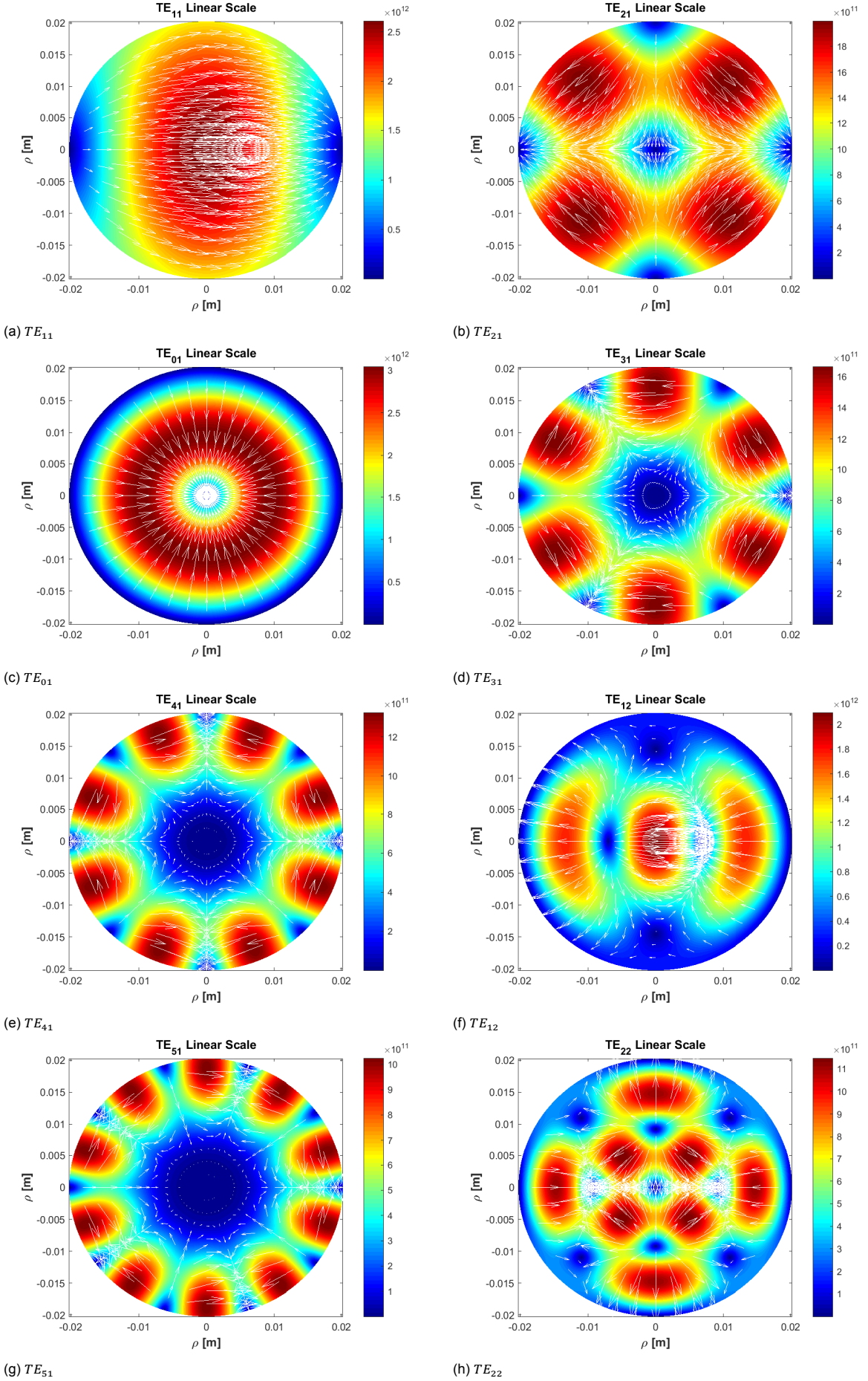


Figure 2.1: E and H fields of TE mode. E field surface plot. H field quiver plot.

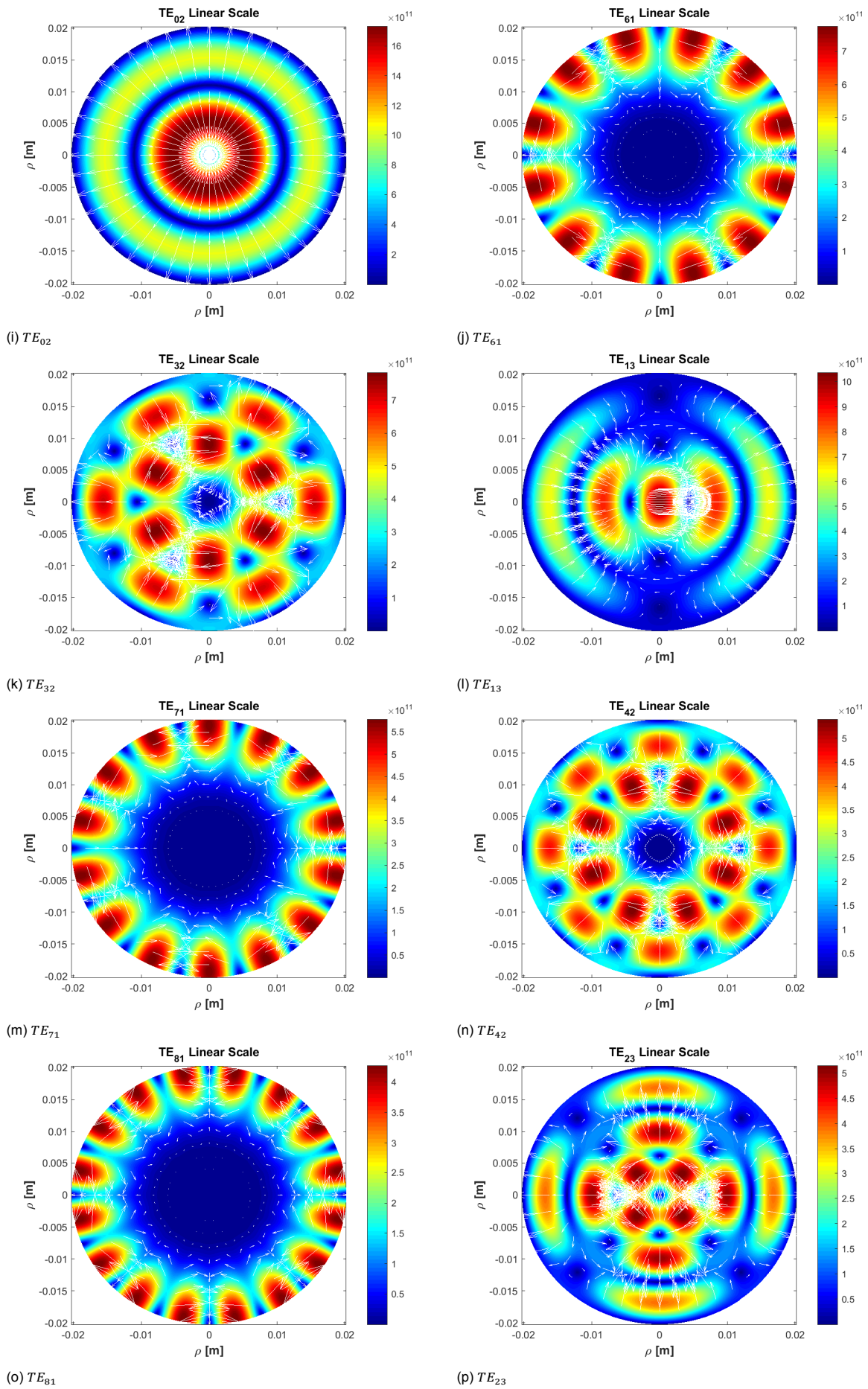


Figure 2.1: E and H fields of TE mode. E field surface plot. H field quiver plot.(cont.)

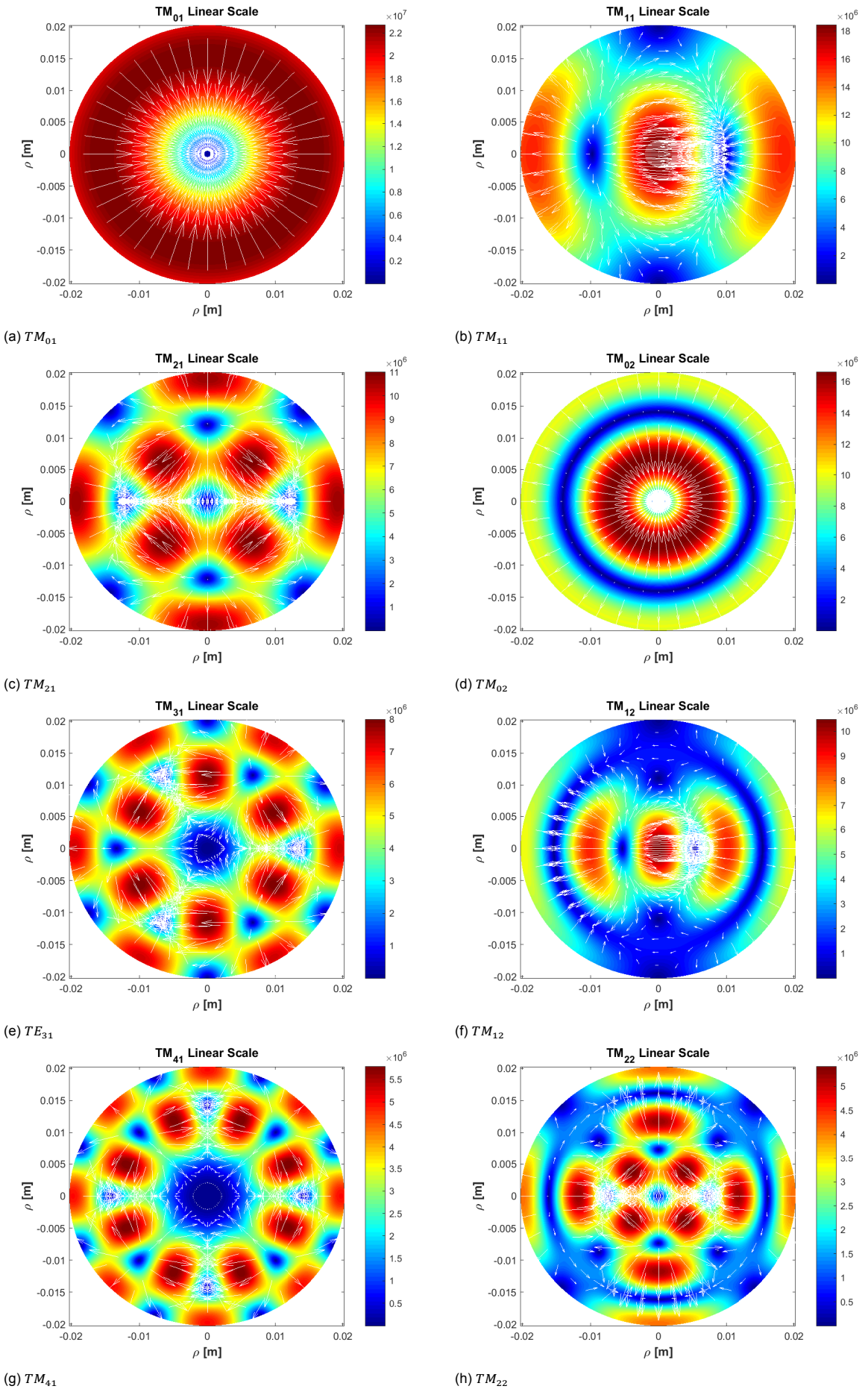


Figure 2.2: E and H fields of TM mode. H field surface plot. E field quiver plot.

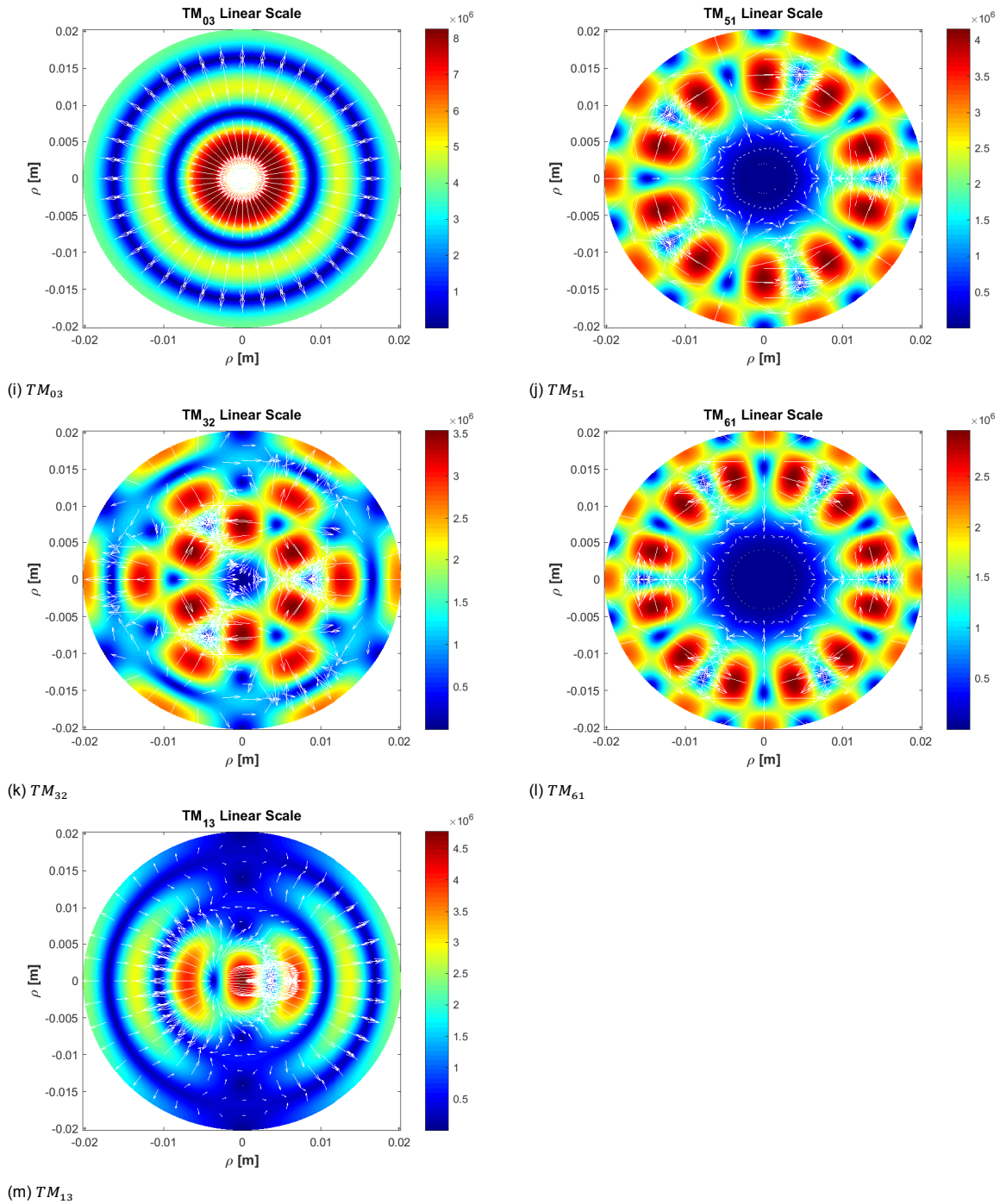


Figure 2.2: E and H fields of TM mode. H field surface plot. E field quiver plot. (Cont.)

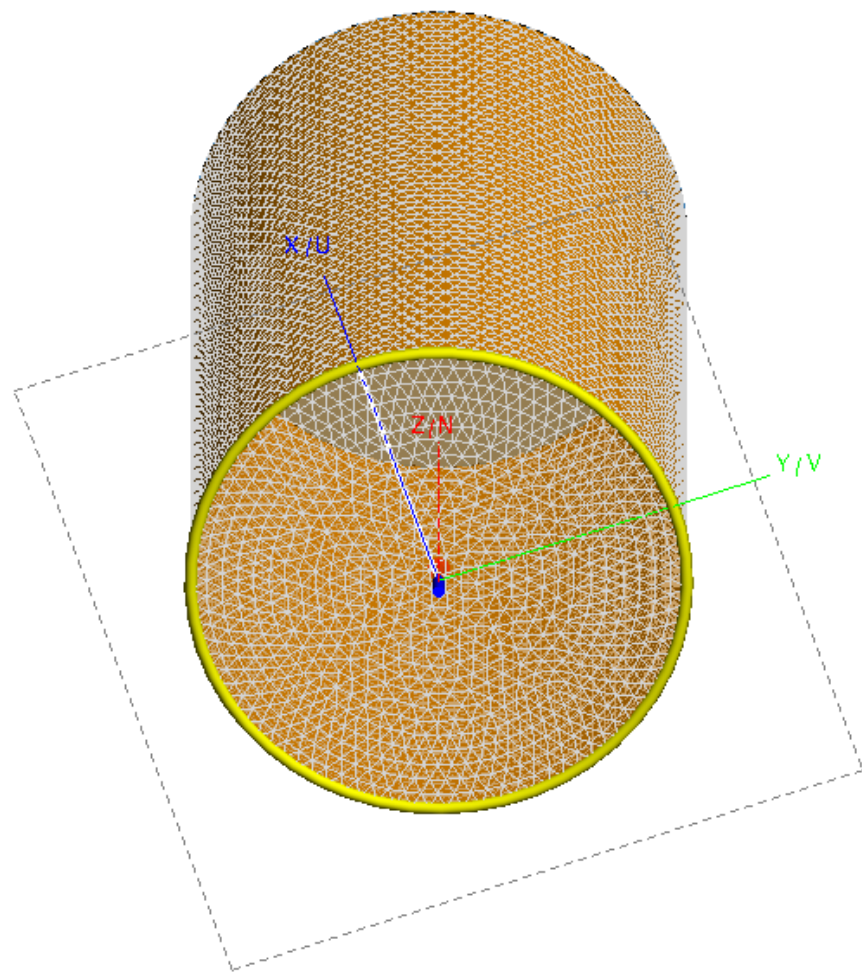


Figure 2.3: Feko Cylinder structure.

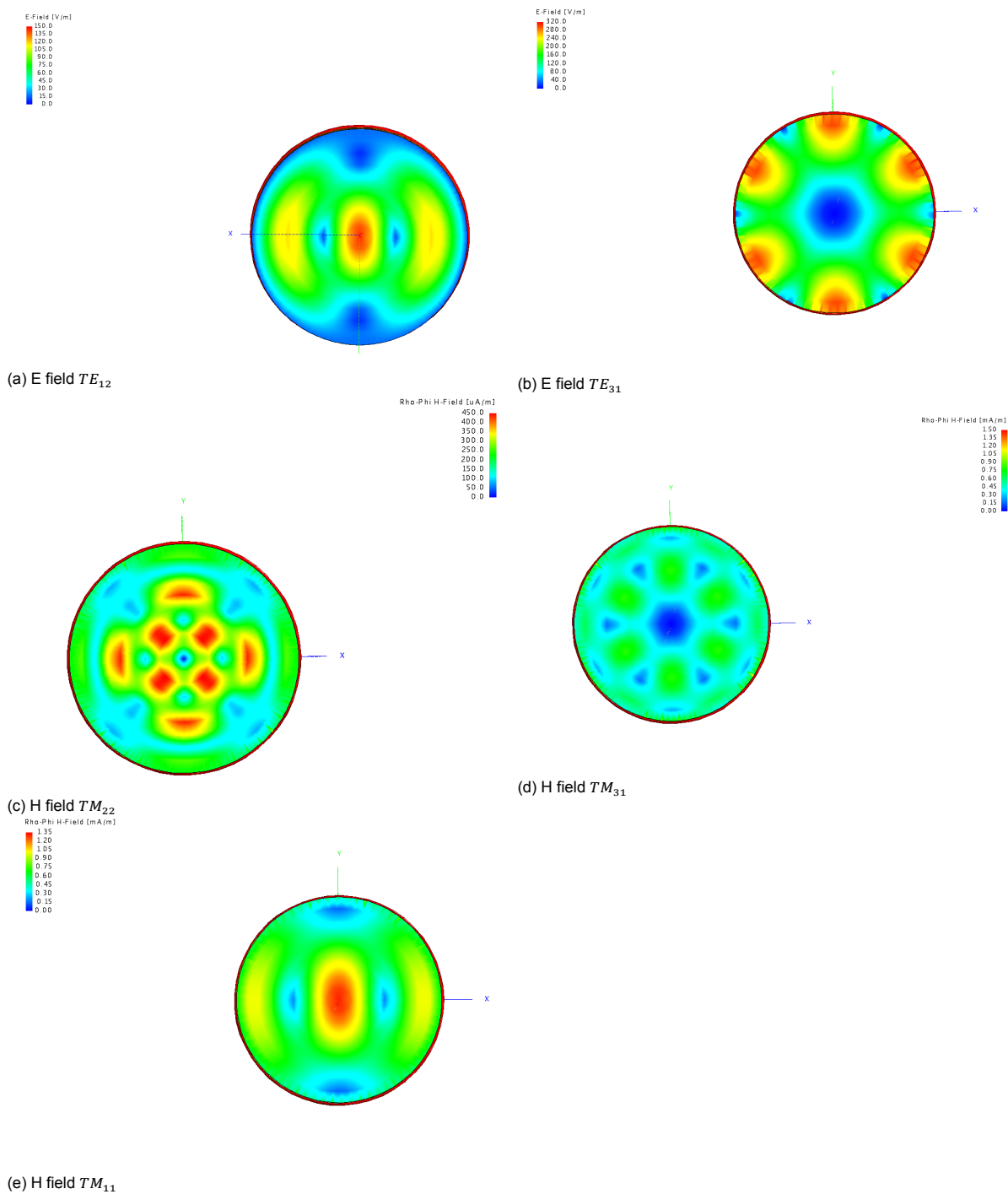


Figure 2.4: E and H fields in Feko for some TE and TM modes.



# 3

## Two Circular Cross-Section Waveguides with Mode Matching Technique

### 3.1. Field Expressions for Circular Cross Section Waveguide

In this chapter, 2 circular cross-section waveguides are studied. They are connected to each other at  $z = 0$ . The problem is shown in figure 3.1.

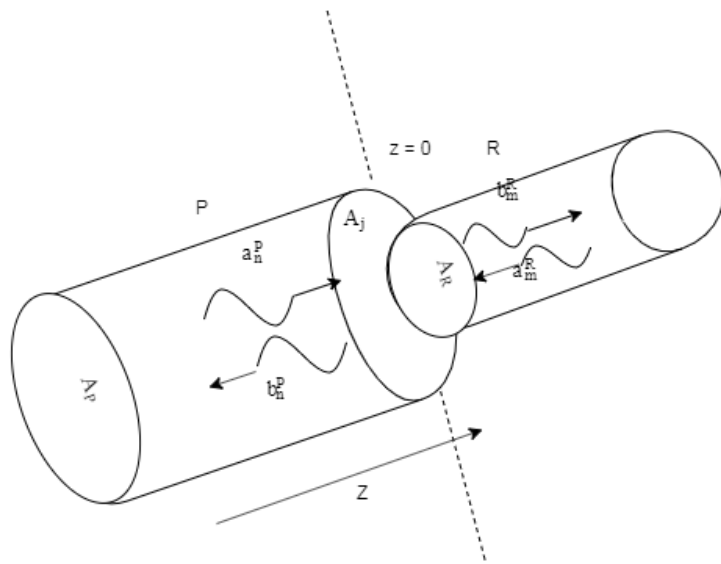


Figure 3.1: Two circular waveguides of different radii connected at  $z = 0$ .

This problem can be solved by determining the GSM (General Scattering Matrix). Here, the two sections at the junctions can be thought as 2 ports and the characteristic of the reflection and transmission coefficients can be determined using the GSM. From previous chapter we already know the field equations for the two waveguides. For the waveguide P, it can be written simply as,

$$\vec{E}_t^P|_{A_P, z=0^-} = \sum_{n=1}^{N_P} (a_n^P + b_n^P) \vec{E}_n^P \quad (3.1)$$

$$\vec{H}_t^P|_{A_P, z=0^-} = \sum_{n=1}^{N_P} (a_n^P - b_n^P) \vec{H}_n^P \quad (3.2)$$

Similarly for the waveguide R, it can be written as,

$$\vec{E}_t^R|_{A_R, z=0^+} = \sum_{m=1}^{N_R} (a_m^R + b_m^R) \vec{E}_n^R \quad (3.3)$$

$$\vec{H}_t^R|_{A_R, z=0^+} = \sum_{m=1}^{N_P} (b_m^R - a_m^R) \vec{H}_n^R \quad (3.4)$$

Here,  $N_P$  and  $N_R$  are the number of modes activated in waveguide P and R respectively. Every mode is orthogonal.

### 3.1.1. Formulation of the Normalization Constant Q for each Mode and its Numerical solution

An arbitrary normalization coefficient for each mode in the waveguides can be calculated by the following relation.

$$\int \int_{A_{area}} (\vec{E}_n^{area} \times \vec{H}_m^{area}) \cdot \hat{z} dS = Q_n^{area} \delta_{nm} \quad (3.5)$$

Here *area* can be both P and R. The  $\delta$  function is 1, when  $m = n$  and 0 otherwise. This explains that the modes are perpendicular.

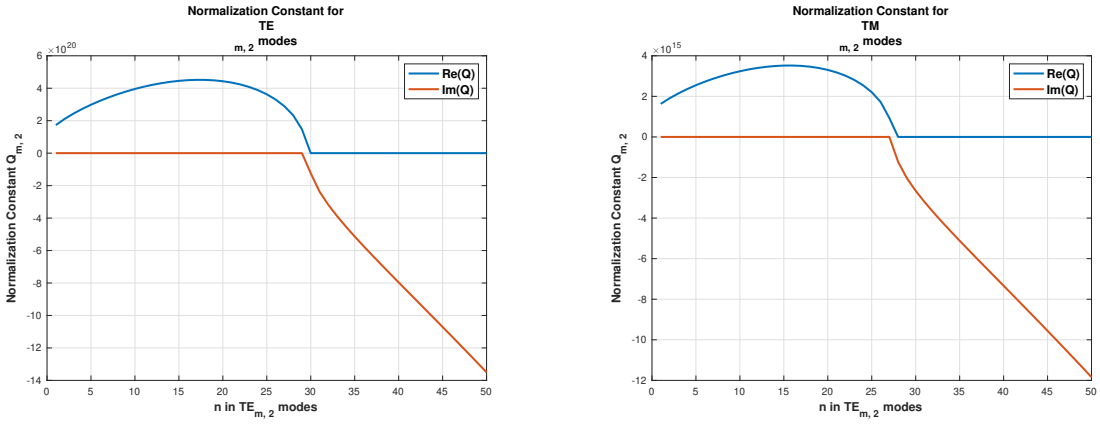
This quantity shows how many modes are propagating and how many are evanescent. It is slightly different from the Poynting vector which is given as:

$$\int \int_{A_{area}} (\vec{E}_n^{area} \times \vec{H}_m^{area}) \cdot \hat{z} dS = Y_m^* \int \int_{A_{area}} (\vec{E}_n^{area} \cdot \vec{E}_m^{area}) dS = Z_n \int \int_{A_{area}} (\vec{H}_n^{area} \cdot \vec{H}_m^{area}) dS = P_n^{area} \delta_{nm} \quad (3.6)$$

Therefore, the normalization constant Q is related to the Poynting vector P as the following:

$$P_n = \frac{\sqrt{Z_n}}{\sqrt{Z_n^*}} |Q_n| \quad (3.7)$$

For verification, the normalization constant Q was plotted at a certain frequency for a number of modes in both TE and TM. The plot is shown in figure 3.2. The double integral is done on the cross-section surface of the waveguide. In this case the double integral looks like  $\int_0^a \int_0^{2\pi}$  to specify the circle in cylindrical coordinates.



(a)  $Q_m$  vs  $m$  in  $TE_{m,2}$  modes

(b)  $Q_m$  vs  $m$  in  $TM_{m,2}$  modes

Figure 3.2: Normalization constant for the modes both in TE and TM

The radius of the waveguide for this simulation was kept as  $r = 2.03[cm]$  and the frequency of operation was 90 GHz. It can be seen from the figure that for the TE modes, at  $TE_{30,2}$ , the

normalization becomes purely imaginary. And before that from  $TE_{2,1}$  to  $TE_{29,2}$ , the normalization was purely real suggesting that there is no real power after  $TE_{29,2}$  mode for 90 GHz. It was found that the cut off for  $TE_{29,2}$  is 88.414 GHz and the cut off for  $TE_{30,2}$  is 90.963 GHz. As the operational frequency was 90 GHz, it couldn't excite modes after  $TE_{30,2}$ . Similarly for TM mode, at  $TE_{28,2}$  mode, the normalization becomes purely imaginary because the cut off at  $TM_{27,2}$  is 88.949 GHz and the cut off at  $TM_{28,2}$  is 91.553 GHz.

### 3.1.2. An analytical approach for Solving for Normalization Constant Q

Using equation (3.5) we have AT Z = 0:

$$Q_n^{area} \delta_{nm} = \int \int_{A_{area}} (\vec{E}_n^{area} \times \vec{H}_m^{area}) \cdot \hat{z} dS = \int \int_{A_{area}} [\vec{E}_{\rho n}^{area} \vec{H}_{\phi m}^{area} - \vec{E}_{\phi n}^{area} \vec{H}_{\rho m}^{area}] \rho d\rho d\phi \quad (3.8)$$

Using equations from chapter 2 (2.23, 2.24, 2.26 and 2.27) for TE modes, we get:

$$Q_n^{area} \delta_{nm} = \int \int_{A_{area}} K_{mnTE} \left[ \frac{m^2}{\rho^2} J_m^2(\beta_{\rho(m,n)} \rho) \sin^2(m\phi) + \beta_{\rho(m,n)}^2 J_m'^2(\beta_{\rho(m,n)} \rho) \cos^2(m\phi) \right] \rho d\rho d\phi \quad (3.9)$$

Where  $K_{mnTE}$  is defined as:

$$K_{mnTE} = \frac{A_{mn}^2 \beta_{z,mn} C_2^2}{\omega \mu \epsilon^2} \quad (3.10)$$

From properties of Bessel's function of the first kind, we know that,

$$J'_v(Z) = \frac{J_{v-1}(Z) - J_{v+1}(Z)}{2} \quad (3.11)$$

And,

$$\frac{2v J_v(Z)}{Z} = J_{v-1}(Z) + J_{v+1}(Z) \quad (3.12)$$

Using these properties the integral can be re-written as:

$$Q_n^{area} \delta_{nm} = K_{mnTE} \frac{\beta_{\rho(m,n)}^2}{4} \left[ (I_A + I_C)(I_{sin} + I_{cos}) + 2I_B(I_{sin} - I_{cos}) \right] \quad (3.13)$$

The terms in the above equation (3.13) are defined as:

$$I_{sin} = \int_0^{2\pi} \sin^2(m\phi) d\phi = \pi \quad (3.14)$$

$$I_{cos} = \int_0^{2\pi} \cos^2(m\phi) d\phi = \pi \quad (3.15)$$

$$I_A = \int_0^r J_{m-1}^2(\beta_{\rho(m,n)} \rho) \rho d\rho \quad (3.16)$$

$$I_B = \int_0^r J_{m-1}(\beta_{\rho(m,n)} \rho) J_{m+1}(\beta_{\rho(m,n)} \rho) \rho d\rho \quad (3.17)$$

$$I_C = \int_0^r J_{m+1}^2(\beta_{\rho(m,n)} \rho) \rho d\rho \quad (3.18)$$

Here, the surface integral is divided into 2 parts; one dependent on  $\rho$  and the other one dependent on  $\phi$ . This was possible because it was assumed in chapter 2 that the field solutions to a cylindrical (circular cross-section) waveguides are a multiplication of independent functions.

$I_A$  and  $I_C$  can be solved analytically by using Lommel's integrals [2] and [7] (Equation 3.19).

$$\int_0^r J_v^2(\beta_{\rho(m,n)} \rho) \rho d\rho = \frac{1}{2} a^2 (J_v(\beta_{\rho(m,n)} a)^2 - J_{v-1}(\beta_{\rho(m,n)} a) J_{v+1}(\beta_{\rho(m,n)} a)); \quad (3.19)$$

However, finding out B is difficult and involves hyper-geometric functions as it has Bessel functions of different orders. However, using equation (3.14) and (3.15) ( $I_{sin} = I_{cos} = \pi$ ), the final integral of equation (3.13) becomes:

$$Q_{nTE}^{area} \delta_{nm} = K_{mnTE} \frac{\beta_{\rho(m,n)}^2}{4} [(I_A + I_C)(I_{sin} + I_{cos})] \quad (3.20)$$

Therefore, the expression with B vanishes.

For TM mode also the solution is identical except the constant  $K_{mnTM}$  which is given as:

$$K_{mnTM} = \frac{B_{mn}^2 \beta_{z,mn} C_2^2}{\omega \mu^2 \epsilon} \quad (3.21)$$

Therefore, the solution is:

$$Q_{nTM}^{area} \delta_{nm} = K_{mnTM} \frac{\beta_{\rho(m,n)}^2}{4} [(I_A + I_C)(I_{sin} + I_{cos})] \quad (3.22)$$

The plots with both numerical and the analytical solution is given in figure 3.3 with  $m = 1$  and  $n$  varying from 1 to 50 at 200 GHz frequency. The analytical result matches the numerical result perfectly. For the numerical result, discretization in  $\rho$  dimension was taken as  $\frac{r}{1000}$  and in  $\phi$  dimension it was  $\frac{\pi}{2000}$ .

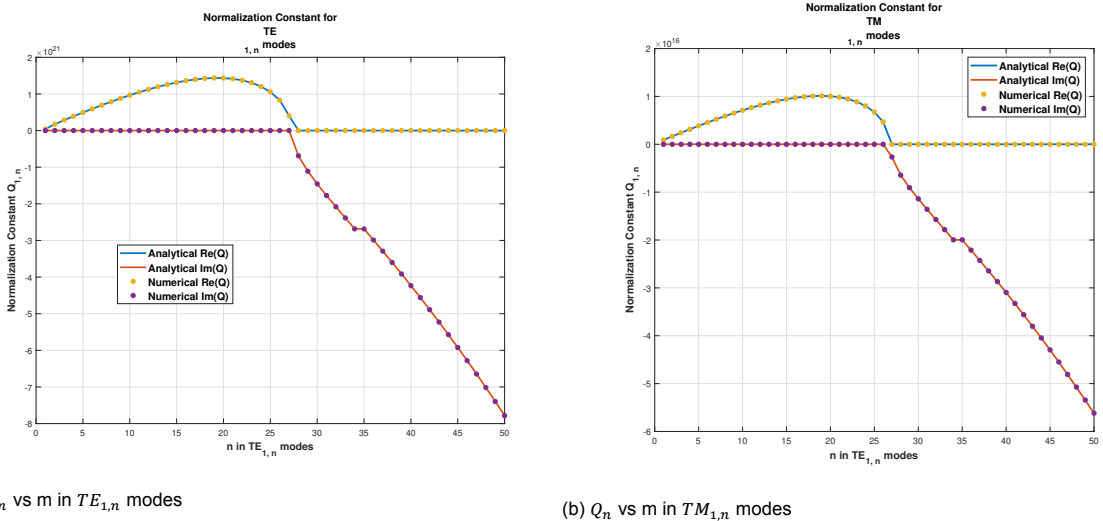


Figure 3.3: Normalization constant for the modes both in TE and TM

### 3.1.3. Mode Matching Technique

Here,  $A_R$  is a subset of  $A_P$  ( $A_P = A_R + A_j$ ) and  $A_j$  is the excess area which is not connected to the waveguide R. The E and H field boundary conditions must be satisfied at the boundary of the 2 waveguides where they are connected.

- For E field:

$$\hat{z} \times \vec{E}^P = 0, \quad \text{in } A_j, z = 0 \quad (3.23)$$

$$\hat{z} \times \vec{E}^P = \hat{z} \times \vec{E}^R, \quad \text{in } A_R, z = 0 \quad (3.24)$$

- For H field:

$$\hat{z} \times \vec{H}^P = \hat{z} \times \vec{H}^R, \quad \text{in } A_R, z = 0 \quad (3.25)$$

For BC of E, we can project it to a magnetic field of all modes in the P waveguide. Therefore,

$$\int \int_{A_P} (\hat{z} \times \vec{E}^P) \cdot \vec{H}_{mode}^P \hat{z} dS = \sum_{n=1}^{N_P} (a_n^P + b_n^P) \int \int_{A_P} (\hat{z} \times \vec{E}_n^P) \cdot \vec{H}_{mode}^P \hat{z} dS \quad (3.26)$$

As the modes are orthogonal to each other this can be rewritten as:

$$\int \int_{A_P} (\hat{z} \times \vec{E}^P) \cdot \vec{H}_{mode}^P \hat{z} dS = (a_{mode}^P + b_{mode}^P) Q_{mode}^P \quad (3.27)$$

The left hand side of equation (3.11) can be calculated by dividing it into 2 sections (one over  $A_R$  and one over  $A_j$ ).

$$\int \int_{A_P} (\hat{z} \times \vec{E}^P) \cdot \vec{H}_{mode}^P \hat{z} dS = \int \int_{A_R} (\hat{z} \times \vec{E}^P) \cdot \vec{H}_{mode}^P \hat{z} dS + \int \int_{A_j} (\hat{z} \times \vec{E}^P) \cdot \vec{H}_{mode}^P \hat{z} dS \quad (3.28)$$

From first BC of E, we know that the second term in the right hand side of the equation (3.13) is 0. Therefore also using the second BC for E,

$$\int \int_{A_P} (\hat{z} \times \vec{E}^P) \cdot \vec{H}_{mode}^P \hat{z} dS = \int \int_{A_R} (\hat{z} \times \vec{E}^R) \cdot \vec{H}_{mode}^P \hat{z} dS = \sum_{m=1}^{N_R} (a_m^R + b_m^R) \int \int_{A_R} \vec{E}_m^R \times \vec{H}_{mode}^P \hat{z} dS \quad (3.29)$$

The term  $\int \int_{A_R} \vec{E}_m^R \times \vec{H}_{mode}^P \hat{z} dS$  is called the inner cross product and it includes the fields in the two waveguides at one integral. Therefore, the above relation can be rewritten as:

$$(a_{mode}^P + b_{mode}^P) Q_{mode}^P = \sum_{m=1}^{N_R} X_{m,mode} (a_m^R + b_m^R) \quad (3.30)$$

This can be calculated for all the modes  $mode = 1, 2, \dots, N_P$ .

Similarly using the magnetic field boundary conditions, we have:

$$\int \int_{A_R} (\hat{z} \times \vec{H}^P) \cdot \vec{E}_{mode}^R \hat{z} dS = \int \int_{A_R} (\hat{z} \times \vec{H}^R) \cdot \vec{E}_{mode}^R \hat{z} dS = Q_{mode}^R (b_{mode}^R - a_{mode}^R) \quad (3.31)$$

$\Rightarrow$

$$\sum_{n=1}^{N_P} X_{mode,n} (a_n^P - b_n^P) = Q_{mode}^R (b_{mode}^R - a_{mode}^R) \quad (3.32)$$

This can be done for all modes  $mode = 1, 2, \dots, N_R$ .

In matrix form the 2 equations can be written as:

$$Q_P (a_P + b_P) = X^t (a_R + b_R) \quad (3.33)$$

$$Q_R (b_R - a_R) = X (a_P - b_P) \quad (3.34)$$

Where,  $Q_P$  and  $Q_R$  are diagonal matrices of order  $N_P \times N_P$  and  $N_R \times N_R$  respectively. And, from definition of the inner cross product X, we know that the dimensions for X should be  $N_R \times N_P$ . From the coefficients  $a_P$  and  $a_R$ ,  $b_P$  and  $b_R$  can be calculated using the Generalised Scattering Matrix (GSM).

$$\begin{bmatrix} b_P \\ b_R \end{bmatrix} = \begin{bmatrix} S_{PP} & S_{PR} \\ S_{RP} & S_{RR} \end{bmatrix} \begin{bmatrix} a_P \\ a_R \end{bmatrix} \quad (3.35)$$

The entries of the GSM matrix can be found by the following,

$$GSM = \begin{bmatrix} Q_P^{-1}X^tFX - I_P & Q_P^{-1}X^tFQ_R \\ FX & FQ_R - I_R \end{bmatrix} \quad (3.36)$$

Here  $I_P$  and  $I_R$  are identity matrices of order  $N_P \times N_P$  and  $N_R \times N_R$  respectively and  $F$  is given by:

$$F = 2(Q_R + XQ_P^{-1}X^t)^{-1} \quad (3.37)$$

**Note:** The projections here mentioned are Galerkin's projections. A Galerkin's projection is made with the same type of quantity. Therefore, for BC of E, for  $\hat{z} \times E$ , a magnetic field is projected and for BC of H, for  $\hat{z} \times H$ , an electric field is projected.

### 3.2. Formulation of the Inner Cross-Product X

First of all the transverse (without the phase term dependent on z) fields can be written as:

**TE:**

$$\vec{E}_n = K_{mnTE}^{\frac{1}{2}} Z_{mnTE}^{\frac{1}{2}} \vec{\Phi}_{En} = K_{mnTE}^{\frac{1}{2}} Z_{mnTE}^{\frac{1}{2}} \nabla_t \Phi_n \times \hat{z} \quad (3.38)$$

$$\vec{H}_n = K_{mnTE}^{\frac{1}{2}} Y_{mnTE}^{\frac{1}{2}} \vec{\Phi}_{Hn} = K_{mnTE}^{\frac{1}{2}} Y_{mnTE}^{\frac{1}{2}} \nabla_t \Phi_n \quad (3.39)$$

$$\vec{E}_{zn} = 0 \quad (3.40)$$

$$\vec{H}_{zn} = -K_{mnTE}^{\frac{1}{2}} Y_{mnTE}^{\frac{1}{2}} \frac{\beta_c^2}{\beta_z} \Phi_n \quad (3.41)$$

Here,  $\Phi_n$  is a scalar function like the potential function described in chapter 2 without the phase term containing z. The  $\Phi_n$ s are the solution to the differential equations of the form  $\Delta_t \Phi_n + \beta_c^2 \Phi_n = 0$ . The expression for the scalar  $\Phi$  function is given as:

$$\Phi_{TE} = J_m(\beta_p \rho) \cos(m\phi) \quad (3.42)$$

**TM:**

$$\vec{H}_n = K_{mnTM}^{\frac{1}{2}} Y_{mnTM}^{\frac{1}{2}} \vec{\Phi}_{Hn} = K_{mnTM}^{\frac{1}{2}} Y_{mnTM}^{\frac{1}{2}} \nabla_t \Phi_n \times \hat{z} \quad (3.43)$$

$$\vec{E}_n = K_{mnTM}^{\frac{1}{2}} Z_{mnTM}^{\frac{1}{2}} \vec{\Phi}_{En} = K_{mnTM}^{\frac{1}{2}} Z_{mnTM}^{\frac{1}{2}} \nabla_t \Phi_n \quad (3.44)$$

$$\vec{H}_{zn} = 0 \quad (3.45)$$

$$\vec{E}_{zn} = -K_{mnTM}^{\frac{1}{2}} Z_{mnTM}^{\frac{1}{2}} \frac{\beta_c^2}{\beta_z} \Phi_n \quad (3.46)$$

The expression for the scalar  $\Phi$  function is given as:

$$\Phi_{TM} = J_m(\beta_\rho \rho) \cos(m\phi) \quad (3.47)$$

The Z and Y are different for TE and TM (Expressions are given in chapter 2).

Using these expressions for the inner cross product, we have:

$$X = \int \int_{A_R} (\vec{E}_{rm,rn}^R \times \vec{H}_{pm,pn}^P) \cdot \hat{z} dS = (K_{rm,rn}^R)^{\frac{1}{2}} (Z_{rm,rn}^R)^{\frac{1}{2}} \bar{X}_{(rm,rn) \rightarrow (pm,pn)} (Y_{pm,pn}^P)^{\frac{1}{2}} (K_{pm,pn}^P)^{\frac{1}{2}} \quad (3.48)$$

Where  $\bar{X}$  is defined as:

$$\bar{X} = \int \int_{A_R} (\vec{\Phi}_{Em}^R \times \vec{\Phi}_{Hn}^P) \cdot \hat{z} dS = \int \int_{A_R} (\vec{\Phi}_{Em}^R \cdot \vec{\Phi}_{En}^P) dS = \int \int_{A_R} (\vec{\Phi}_{Hm}^R \cdot \vec{\Phi}_{Hn}^P) dS \quad (3.49)$$

Therefore, the matrix  $\bar{X}$  is frequency independent. It can be solved with surface integrals over the domain  $A_R$ . The simplifications to this integral can be found by the following formulae:

**TE mode in P and TE mode in R** Following equations (3.32) and (3.24)

$$\bar{X} = \int \int_{A_R} (\vec{\Phi}_{Hm}^R \cdot \vec{\Phi}_{Hn}^P) dS = \int \int_{A_R} \nabla_t \Phi_R \cdot \nabla_t \Phi_P dS \quad (3.50)$$

**TE mode in P and TM mode in R** Following equations (3.32) and (3.24)

$$\bar{X} = \int \int_{A_R} (\vec{\Phi}_{Em}^R \times \vec{\Phi}_{Hn}^P) \cdot \hat{z} dS = \int \int_{A_R} (\nabla_t \Phi_R \times \nabla_t \Phi_P) \cdot \hat{z} dS = 0 \quad (3.51)$$

**TM mode in P and TE mode in R**

$$\bar{X} = \int \int_{A_R} (\vec{\Phi}_{Em}^R \times \vec{\Phi}_{Hn}^P) \cdot \hat{z} dS = \int \int_{A_R} (\nabla_t \Phi_R \times \nabla_t \Phi_P) \cdot \hat{z} dS \quad (3.52)$$

**TM mode in P and TM mode in R**

Following equations (3.32) and (3.30)

$$\bar{X} = \int \int_{A_R} (\vec{\Phi}_{Em}^R \cdot \vec{\Phi}_{En}^P) dS = \int \int_{A_R} \nabla_t \Phi_R \cdot \nabla_t \Phi_P dS \quad (3.53)$$

### 3.2.1. Formulation of Inner Cross Product using Normalized Field Equations

The potential function used in the previous formulation wasn't normalized. There is another way to visualise the problem with normalized field equations where the potentials can be written as:

$$\Psi = (N_{TE/TM}) J_m(\beta_\rho \rho) \cos(m\phi) \quad (3.54)$$

The potential function is a solution to the differential equation  $\Delta_t \Psi_n + \beta_\rho^2 \Psi_n = 0$  with the boundary condition that:

$$\int \int_S |\nabla_t \Psi_n|^2 dS = 1 \quad (3.55)$$

Applying the boundary condition of orthogonality, we can find the normalization factor. The above equation 3.55 can be rewritten as:

$$(N_{TE/TM})^2 \int \int_{A_{area}} \left[ \frac{m^2}{\rho^2} J_m^2(\beta_{\rho(m,n)} \rho) \sin^2(m\phi) + \beta_{\rho(m,n)}^2 J_m'^2(\beta_{\rho(m,n)} \rho) \cos^2(m\phi) \right] \rho d\rho d\phi = 1 \quad (3.56)$$

Here, the integral exactly looks like the integral that appeared in the normalization factor  $Q$  in section 3.1.2 equation (3.9). Therefore, the solution as per equation 3.20 is:

$$\int \int_S |\nabla_t \Psi_n|^2 dS = (N_{TE/TM})^2 \frac{\beta_{\rho(m,n)}^2}{4} (I_A + I_C) 2\pi \quad (3.57)$$

$I_A$  and  $I_C$  are given in the equations 3.16 and 3.18. Using Lommel's integral of equation 3.19, we can further simplify the term  $I_A + I_C$  as,

### For TE

We know that for TE,

$$J'_m(\beta_\rho r) = 0 \quad (3.58)$$

$\Rightarrow$

Using the Bessel's function properties,

$$J_{m-1}(\beta_\rho r) = J_{m+1}(\beta_\rho r) \quad (3.59)$$

$$J_{m-1}(\beta_\rho r) = \frac{m}{\beta_\rho r} J_m(\beta_\rho r) \quad (3.60)$$

Using these properties, it is found that,

$$I_A + I_C = \frac{1}{2} r^2 \frac{J_m^2(\beta_\rho r)}{(\beta_\rho r)^2} 2((\beta_\rho r)^2 - m^2) = \frac{J_m^2(\beta_\rho r)}{(\beta_\rho)^2} ((\beta_\rho r)^2 - m^2) \quad (3.61)$$

Using this on equation 3.57, we have,

$$\int \int_S |\nabla_t \Psi_n|^2 dS = (N_{TE})^2 \frac{\beta_{\rho(m,n)}^2}{4} (I_A + I_C) 2\pi = \frac{\pi}{2} J_m^2(\beta_\rho r) ((\beta_\rho r)^2 - m^2) = 1 \quad (3.62)$$

$\Rightarrow$

$$N_{TE} = \frac{\sqrt{\frac{2}{\pi}}}{J_m(\beta_{\rho(m,n)} r) \sqrt{((\beta_{\rho(m,n)} r)^2 - m^2)}} \quad (3.63)$$

The term  $\beta_{\rho(m,n)} r$  is just the  $n$ th root of the derivative of the  $m$ th order Bessel function which is written in chapter 2 as ( $\chi'_{mn}$ )

$$N_{TE} = \frac{\sqrt{\frac{2}{\pi}}}{J_m(\chi'_{mn}) \sqrt{(\chi'^2_{mn} - m^2)}} \quad (3.64)$$

### For TM

For TM using the property that  $J_m(\beta_\rho r) = 0$  and the boundary condition of the normalized power (3.55), it is found that,

$$N_{TM} = \frac{\sqrt{\frac{2}{\pi}}}{J'_m(\chi_{mn}) \chi_{mn}} \quad (3.65)$$

The term  $\beta_{\rho(m,n)} r$  for TM is just the  $n$ th root of the  $m$ th order Bessel function which is written in chapter 2 as ( $\chi_{mn}$ )

Using this normalized potential scalar function  $\Psi$ , the equations from 3.38 to 3.47 can be rewritten as, **TE:**

$$\vec{E}_n = Q_{mnTE}^{\frac{1}{2}} Z_{mnTE}^{\frac{1}{2}} \vec{\Psi}_{En} = Q_{mnTE}^{\frac{1}{2}} Z_{mnTE}^{\frac{1}{2}} \nabla_t \Psi_n \times \hat{z} \quad (3.66)$$

$$\vec{H}_n = Q_{mnTE}^{\frac{1}{2}} Y_{mnTE}^{\frac{1}{2}} \vec{\Psi}_{Hn} = Q_{mnTE}^{\frac{1}{2}} Y_{mnTE}^{\frac{1}{2}} \nabla_t \Psi_n \quad (3.67)$$

$$\vec{E}_{zn} = 0 \quad (3.68)$$

$$\vec{H}_{zn} = -Q_{mnTE}^{\frac{1}{2}} Y_{mnTE}^{\frac{1}{2}} \frac{\beta_c^2}{\beta_z} \Psi_n \quad (3.69)$$

The expression for the scalar  $\Psi$  function is given as: (As listed in the Appendix of [5])

$$\Psi_{TE} = (N_{TE}) J_m(\beta_\rho \rho) \cos(m\phi) \quad (3.70)$$

**TM:**

$$\vec{H}_n = Q_{mnTM}^{\frac{1}{2}} Y_{mnTM}^{\frac{1}{2}} \vec{\Psi}_{Hn} = Q_{mnTM}^{\frac{1}{2}} Y_{mnTM}^{\frac{1}{2}} \nabla_t \Psi_n \times \hat{z} \quad (3.71)$$

$$\vec{E}_n = Q_{mnTM}^{\frac{1}{2}} Z_{mnTM}^{\frac{1}{2}} \vec{\Psi}_{En} = Q_{mnTM}^{\frac{1}{2}} Z_{mnTM}^{\frac{1}{2}} \nabla_t \Psi_n \quad (3.72)$$

$$\vec{H}_{zn} = 0 \quad (3.73)$$

$$\vec{E}_{zn} = -Q_{mnTM}^{\frac{1}{2}} Z_{mnTM}^{\frac{1}{2}} \frac{\beta_c^2}{\beta_z} \Psi_n \quad (3.74)$$

The expression for the scalar  $\Psi$  function is given as: (As listed in the Appendix of [5])

$$\Psi_{TM} = (N_{TM}) J_m(\beta_\rho \rho) \cos(m\phi) \quad (3.75)$$

The difference between equations 3.38 to 3.47 and 3.66 to 3.75 is that the  $K_{mn}$  terms are replaced by the normalization constant (conjugate power terms)  $Q_{mn}$  and  $\Phi$  is replaced by  $\Psi$ . Here, the potential function  $\Psi$  is different for TE and TM.

Using this normalized potentials, the inner product is defined as:

$$X = \int \int_{A_R} (\vec{E}_{rm,rn}^R \times \vec{H}_{pm,pn}^P) \cdot \hat{z} dS = (Q_{rm,rn}^R)^{\frac{1}{2}} (Z_{rm,rn}^R)^{\frac{1}{2}} X_{\Psi(rm,rn) \rightarrow (pm,pn)} (Y_{pm,pn}^P)^{\frac{1}{2}} (Q_{pm,pn}^P)^{\frac{1}{2}} \quad (3.76)$$

Where  $X_\Psi$  is defined as:

$$\bar{X}_\Psi = \int \int_{A_R} (\vec{\Psi}_{Em}^R \times \vec{\Psi}_{Hn}^P) \cdot \hat{z} dS = \int \int_{A_R} (\vec{\Psi}_{Em}^R \cdot \vec{\Psi}_{En}^P) dS = \int \int_{A_R} (\vec{\Psi}_{Hm}^R \cdot \vec{\Psi}_{Hn}^P) dS \quad (3.77)$$

### 3.2.2. Analytical Formulation of the Inner Cross Product for modes TE, TE and TM, TM combination

The analytical formulation can be done using the same principles mentioned for the normalization constant Q in the previous sub-section. Using equation (3.50), we have:

**For TE and TE / For TM and TM**

$$\bar{X} = \int \int_{A_R} \nabla_t \Phi_R \cdot \nabla_t \Phi_P dS = \frac{\beta_{\rho(pm,pn)} \beta_{\rho(rm,rn)}}{4} \left[ (I_A + I_D)(I_{cos} + I_{sin}) - (I_B + I_C)(I_{cos} - I_{sin}) \right] \quad (3.78)$$

Where pm and pn are the mode numbers for the waveguide P and rm and rn are the mode number for the waveguide R.

Here, to make it simple, pm and rm are kept the same. (In the plots pm = rm = 1) to have a simplified analytical solution for the inner cross product.

The integrals mentioned in the equation are::

$$I_{sin} = \int_0^{2\pi} \sin(pm\phi) \sin(rm\phi) d\phi = \pi, \quad pm = rm \quad (3.79)$$

$$I_{cos} = \int_0^{2\pi} \cos(pm\phi) \cos(rm\phi) d\phi = \pi, \quad pm = rm \quad (3.80)$$

$$I_A = \int_0^r J_{pm-1}(\beta_{\rho(pm,pn)}\rho) J_{rm-1}(\beta_{\rho(rm,rn)}\rho) \rho d\rho \quad (3.81)$$

$$I_B = \int_0^r J_{pm-1}(\beta_{\rho(pm,pn)}\rho) J_{rm+1}(\beta_{\rho(rm,rn)}\rho) \rho d\rho \quad (3.82)$$

$$I_C = \int_0^r J_{pm+1}(\beta_{\rho(pm,pn)}\rho) J_{rm-1}(\beta_{\rho(rm,rn)}\rho) \rho d\rho \quad (3.83)$$

$$I_D = \int_0^r J_{pm+1}(\beta_{\rho(pm,pn)}\rho) J_{rm+1}(\beta_{\rho(rm,rn)}\rho) \rho d\rho \quad (3.84)$$

$I_A$  and  $I_D$  can be solved with Lommel's integrals [2] and [7].

$$\int_0^r J_\nu(\beta_\nu \rho) J_\nu(\beta_\mu \rho) \rho d\rho = \frac{r}{(\beta_\nu^2 - \beta_\mu^2)} \left( -\beta_\nu J_{\nu-1}(\beta_\nu r) J_\nu(\beta_\mu r) + \beta_\mu J_\nu(\beta_\nu r) J_{\nu-1}(\beta_\nu r) \right) \quad (3.85)$$

However, B and C have complicated analytical solutions involving hyper-geometric functions.

However, as when  $pm = rm$ , in the original expression of equation (3.76), the term with B + C vanishes because  $I_{sin} = I_{cos} = \pi$ . Therefore, the inner cross product becomes:

$$\bar{X} = \int \int_{A_R} \nabla_t \Phi_R \cdot \nabla_t \Phi_P dS = \frac{\beta_{\rho(pm,pn)} \beta_{\rho(rm,rn)}}{4} \left[ (I_A + I_D)(I_{cos} + I_{sin}) \right] \quad (3.86)$$

### 3.3. Convergence of Mode Matching Technique

Convergence of the mode matching technique was studied by adding more modes on the input section keeping the ratio of the number of modes as the aspect ratio (in this case the ratio of the areas of the two different cross-sections for the 2 waveguides).

#### Example 1

The first test was done when the radii of waveguide P and R are almost the same.

( $r_p = 2[cm]$ ,  $r_r = 1.9[cm]$ ). As the radii are almost the same the convergence study was carried out by fixing the ratio of number of modes as 1 and increasing the number of modes. The results are shown in figure 3.4. The frequency was chosen to be a frequency with which all modes that are included are propagating modes on both waveguides. The plot shows the various S parameters of the fundamental mode only.

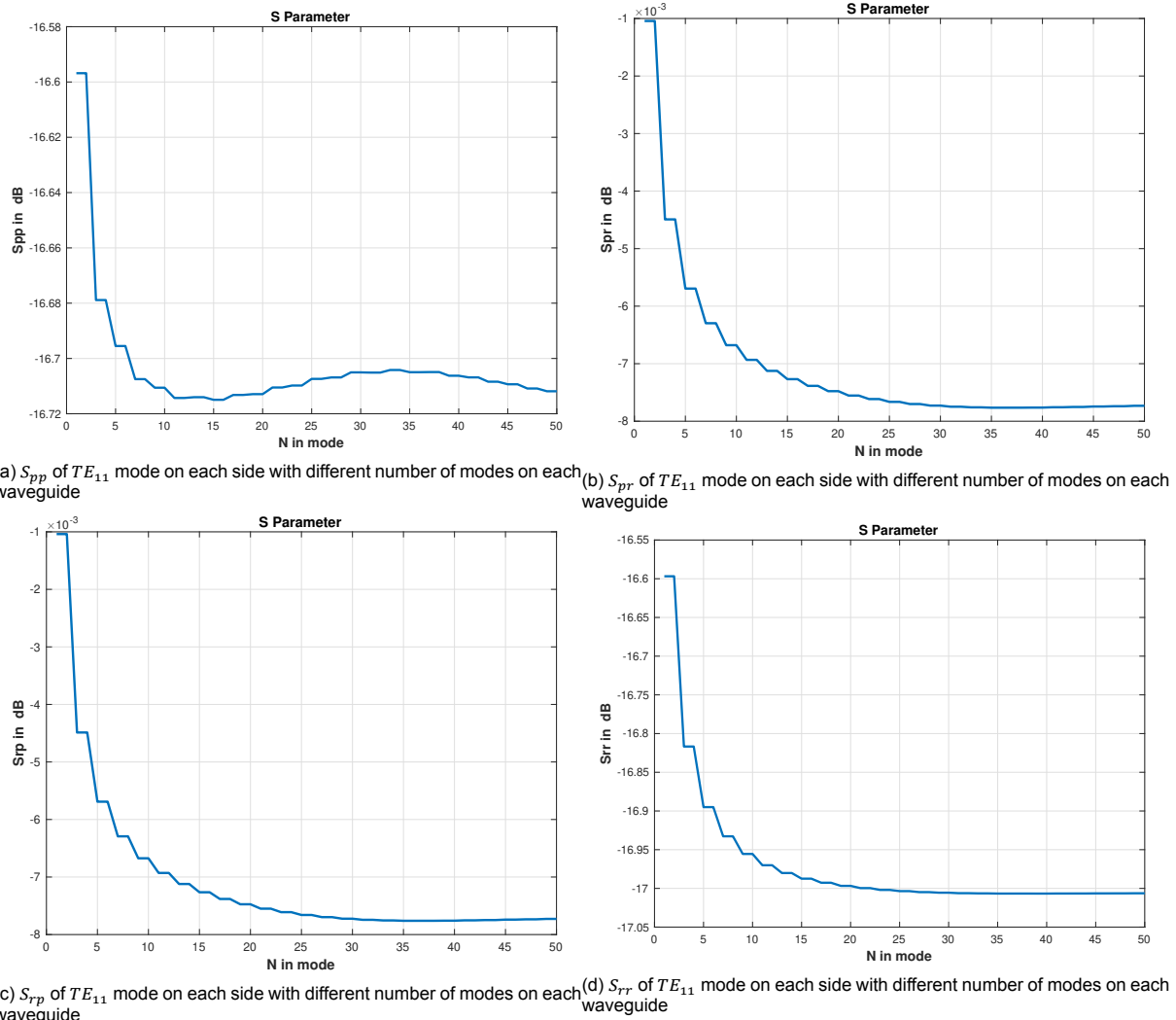


Figure 3.4: Convergence study when radii ratio is approximately 1.

The figure 3.4 suggests that the convergence of results occurs when we include higher order modes till 25 or more on both waveguides. The relative convergence criterion is explained in [3] and [4]. The relative convergence criterion is important in convergence study. Only increasing the number of modes doesn't help in increasing accuracy unless the ratio of number of modes on both the sides is appropriate.

### Example 2

The same convergence study is carried out but with a different set of radii than in example 1. The radii were chosen to be  $r_p = 2[cm]$  and  $r_r = 1[cm]$ . Therefore, the ratio of the areas become  $\frac{\pi r_p^2}{\pi r_r^2} = 4$ . The results are shown in figure 3.5. Here, the modes on the x axes are the modes represented by the modes in the smaller waveguide R. The larger waveguide P has 4 times more modes than the smaller waveguide R. It is seen that after 10 modes in R (40 modes in P), the S parameter values are converging.

The convergence for example 1 can be explained in the below figure 3.6 where  $S_{pp}$  is plotted for  $TE_{11}$  mode. Better results are seen when higher order modes are considered. Similarly the comparison is done with results from Feko. The comparison is done till 10 modes on each side as for number of modes more than 10, the CPU time is too high. In both cases (MM and Feko), the dip at 6.5 GHz becomes smaller and smaller with increasing number of modes, which shows the importance of including higher order modes into the analysis. The comparison done in Feko simulations is shown in figure 3.7. It is seen that with MM technique, this convergence is faster than Feko simulations.

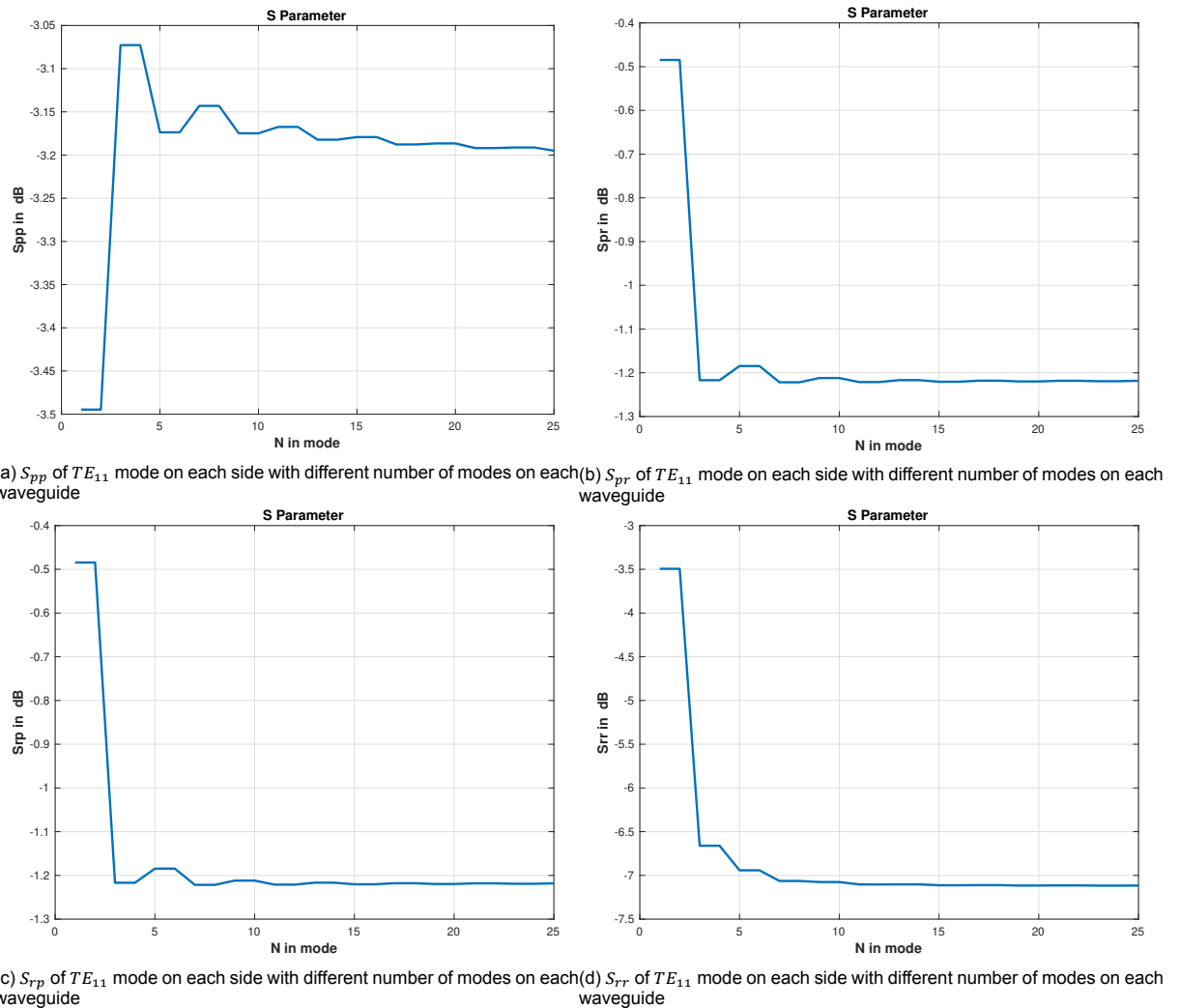


Figure 3.5: Convergence study when radii ratio is 2.

### 3.3.1. Feko Simulations and Comparison

Example 1 stated above was simulated on Feko. The results are shown in figure 3.8 along with the results of the MATLAB model using the mode matching techniques mentioned above. Here, the number of modes on each waveguide is 10. Beyond that with a Method of Moments solver on Feko, the time of simulation is very high.

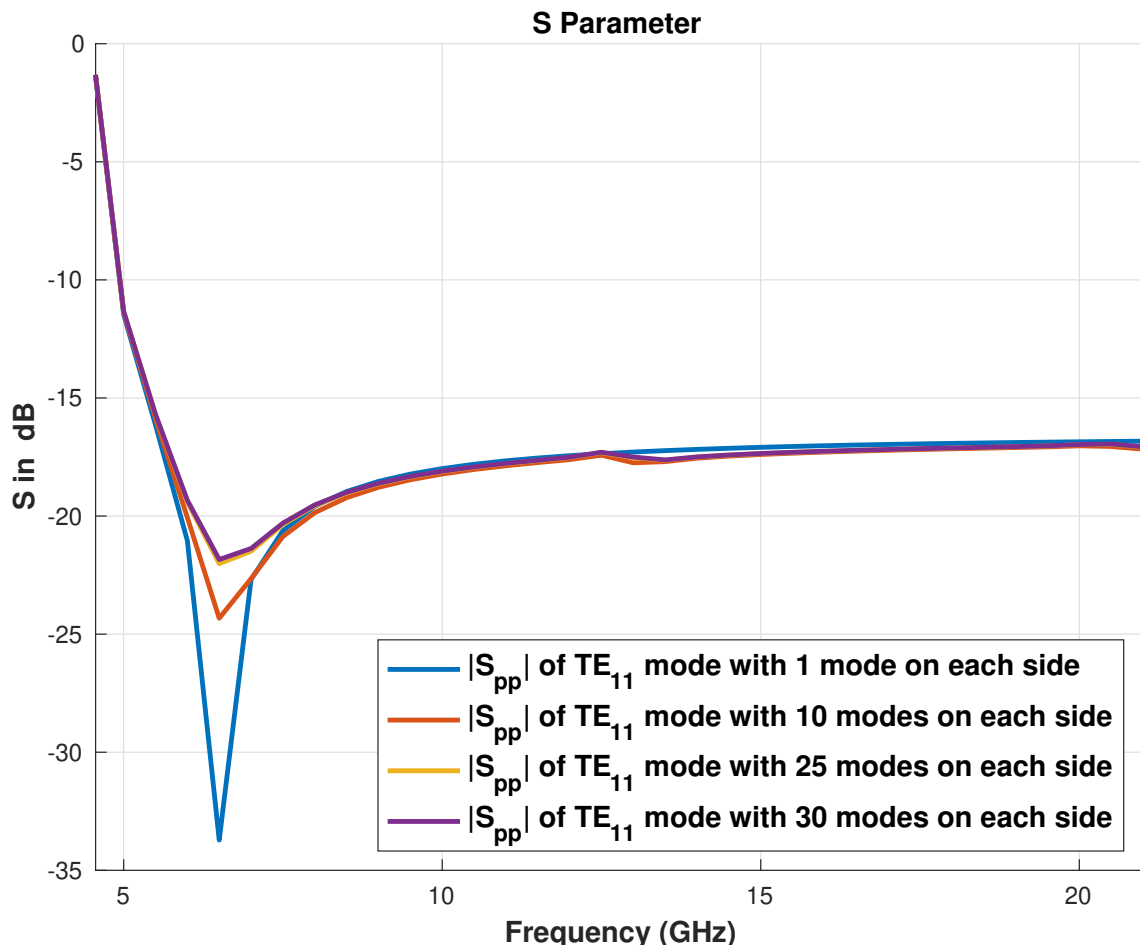


Figure 3.6:  $S_{pp}$  for  $TE_{11}$  modes with different number of modes on each waveguide using MM technique. Ratio of number of modes on each side is kept as 1.

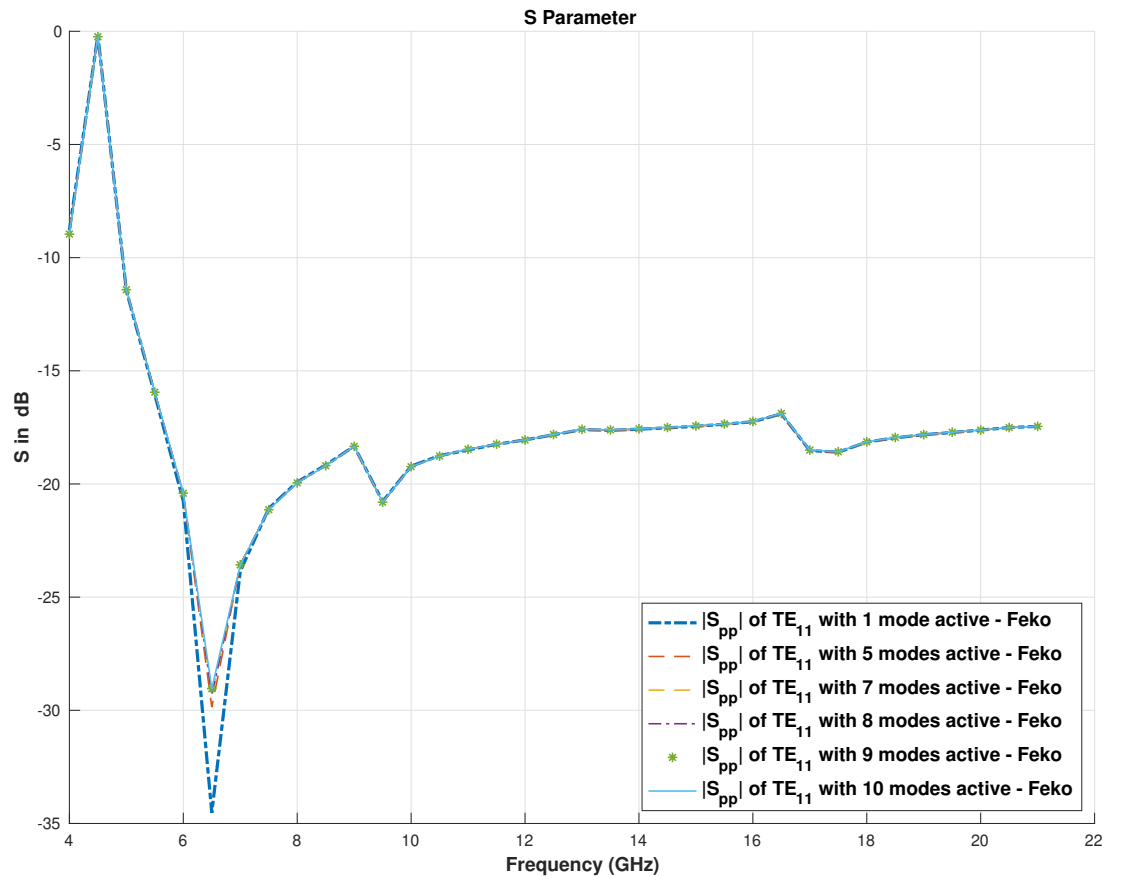
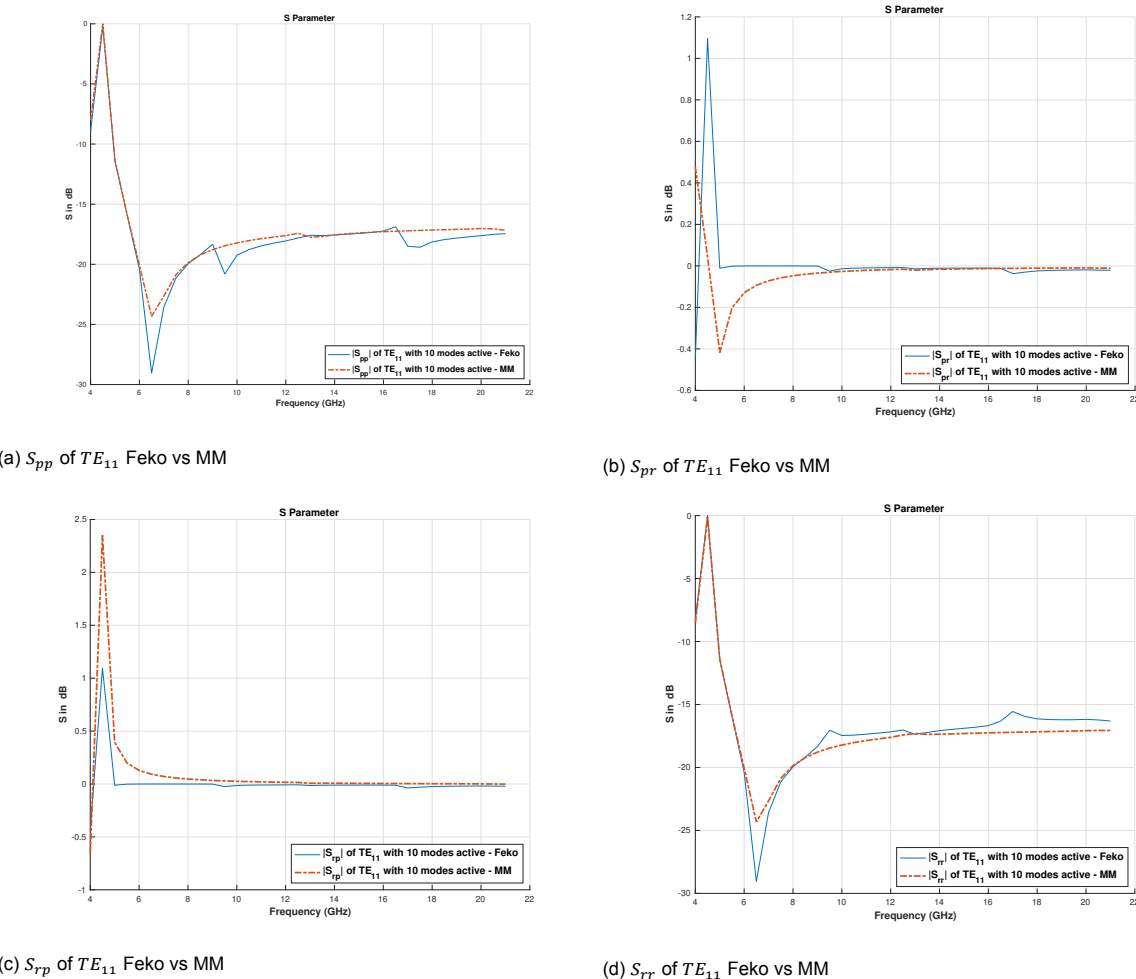


Figure 3.7:  $S_{pp}$  for  $TE_{11}$  modes with different number of modes on each waveguide from Feko simulations. Ratio of number of modes on each side is kept as 1.

Figure 3.8: S parameters for  $TE_{11}$  mode - Feko vs MM. 10 modes active on each waveguide



# 4

## Cascaded Circular Cross-Section Waveguides with Mode Matching Technique

In the previous chapter, only 2 waveguides were studied with one GSM matrix. This chapter covers the formulation of the scattering matrix when a number of waveguides are connected in a row. As in the previous section the GSM was found at  $z = 0$ , the phase term of  $e^{-j\beta_z l}$  didn't come into picture. As  $z$  dependence doesn't affect the magnitude of S parameters, it was ignored. However, in a cascaded structure, the phase information is important as the discontinuities are at different points over the  $z$  axis. As described in [6], we first consider a simple structure with 3 waveguides. The 2 waveguides remain the same as in the previous chapter and one bigger waveguide T is cascaded after the waveguide P on the negative  $z$  axis. Therefore, the port on the outer surface of P is now translated to the outer surface of T. The figure 4.1 shows the Geometry and figure 4.2 shows the circuit structure with GSM matrices of each junction. Figure 4.3 shows the equivalent circuit representation with one equivalent GSM.

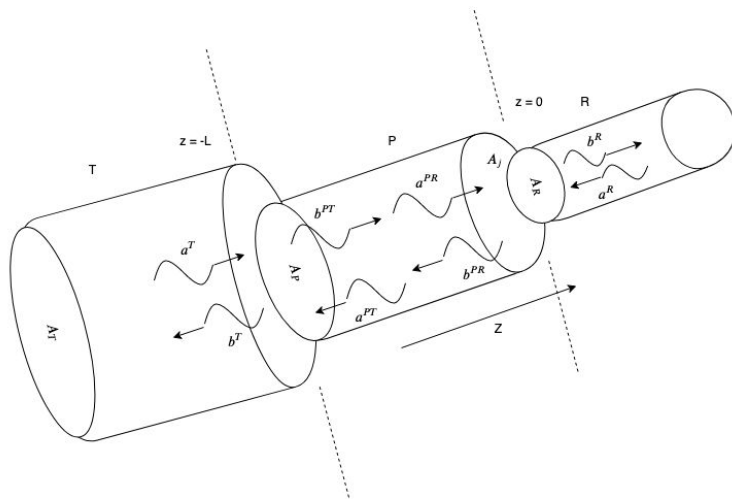


Figure 4.1: 3 waveguides configuration. 2 discontinuities.

### 4.1. Formulation of GSM

Based on section 3.1.3, we can write the matrix form equations for all the three regions as:

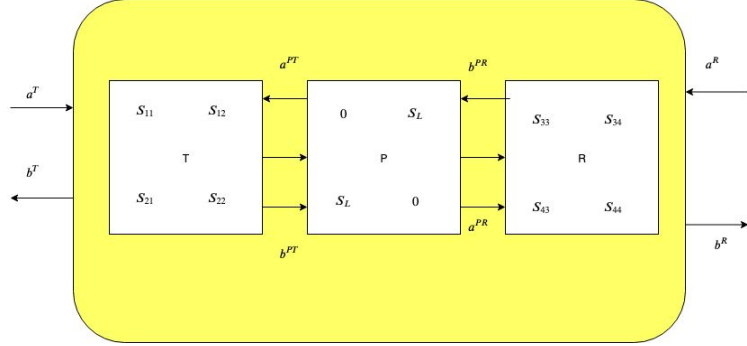


Figure 4.2: 3 waveguides CCT configuration. 2 discontinuities.

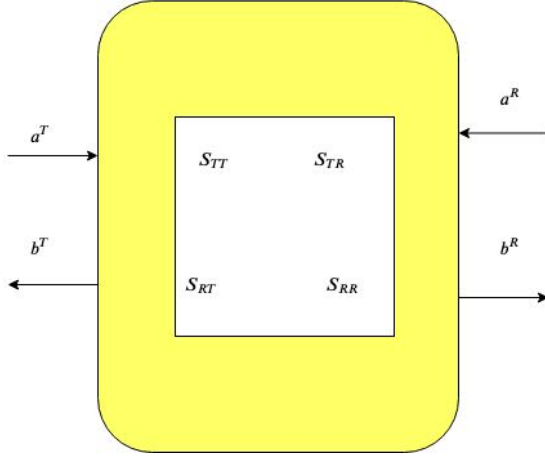


Figure 4.3: 3 waveguides equivalent CCT configuration. 2 discontinuities.

$$\begin{bmatrix} b_T \\ b_{PT} \end{bmatrix} = \begin{bmatrix} S_{11} & S_{12} \\ S_{21} & S_{22} \end{bmatrix} \begin{bmatrix} a_T \\ a_{PT} \end{bmatrix} \quad (4.1)$$

$$\begin{bmatrix} a_{PT} \\ a_{PR} \end{bmatrix} = \begin{bmatrix} 0 & S_L \\ S_L & 0 \end{bmatrix} \begin{bmatrix} b_{PT} \\ b_{PR} \end{bmatrix} \quad (4.2)$$

And,

$$\begin{bmatrix} b_{PR} \\ b_R \end{bmatrix} = \begin{bmatrix} S_{33} & S_{34} \\ S_{43} & S_{44} \end{bmatrix} \begin{bmatrix} a_{PR} \\ a_R \end{bmatrix} \quad (4.3)$$

Equations 4.1 and 4.2 yield,

$$b_T = S_{11}a_T + S_{12}S_Lb_{PR} \quad (4.4)$$

$$b_{PT} = S_{21}a_T + S_{22}S_Lb_{PR} \quad (4.5)$$

Equations 4.2 and 4.3 yield,

$$b_{PR} = S_{33}S_Lb_P + S_{34}a_R \quad (4.6)$$

$$b_R = S_{43}S_Lb_{PT} + S_{44}a_R \quad (4.7)$$

Solving 4.5 and 4.6 we have,

$$b_{PT} = U_1(S_{21}a_T + S_{22}S_L S_{34}a_R) \quad (4.8)$$

$$b_{PR} = U_2(S_{33}S_L S_{21}a_T + S_{44}a_R) \quad (4.9)$$

Where,

$$U_1 = (I - S_{22}S_L S_{33}S_L)^{-1} \quad (4.10)$$

And,

$$U_2 = (I - S_{33}S_L S_{22}S_L)^{-1} \quad (4.11)$$

Using 4.8 and 4.9 on 4.4 and 4.7, we have,

$$b_T = (s_{11} + S_{12}S_L U_2 S_{33}S_L S_{21})a_T + S_{12}S_L U_2 S_{34}a_R \quad (4.12)$$

$$b_R = (s_{44} + S_{43}S_L U_1 S_{22}S_L S_{34})a_R + S_{43}S_L U_1 S_{21}a_T \quad (4.13)$$

Therefore GSM is given by,

$$\begin{bmatrix} S_{TT} & S_{TR} \\ S_{RT} & S_{RR} \end{bmatrix} = \begin{bmatrix} s_{11} + S_{12}S_L U_2 S_{33}S_L S_{21} & S_{12}S_L U_2 S_{34} \\ S_{43}S_L U_1 S_{21} & s_{44} + S_{43}S_L U_1 S_{22}S_L S_{34} \end{bmatrix} \quad (4.14)$$

Here,  $S_L$  is a diagonal matrix with elements which are phase terms which depend on z and the wavenumber  $\beta_z$ . Each diagonal element is for each mode.

$$S_L = \begin{bmatrix} e^{-j\beta_{z1}L} & 0 & 0 & 0 & \dots & 0 \\ 0 & e^{-j\beta_{z2}L} & 0 & 0 & \dots & 0 \\ 0 & 0 & e^{-j\beta_{z3}L} & 0 & \dots & 0 \\ \vdots & \vdots & \vdots & \vdots & \ddots & \vdots \\ \vdots & \vdots & \vdots & \vdots & \ddots & \vdots \\ 0 & 0 & \vdots & \vdots & \ddots & e^{-j\beta_{zN}L} \end{bmatrix} \quad (4.15)$$

Here  $e^{-j\beta_{zi}L}$  is the wavenumber for the mode  $i$ .

#### 4.1.1. Convergence with 3 waveguide structure

The waveguide structure that was simulated in MATLAB and Feko is shown in figure 4.4. The radius of the three waveguides are ( $r_r = 1.93$  [cm],  $r_p = 2.03$  [cm],  $r_t = 2.13$  [cm]). The waveguide length of the R waveguide in between the P and T is 2 [cm].

The convergence obtained from the 3 waveguide structure with Mode Matching Technique is shown in figure 4.5a and a zoomed in figure is shown in figure 4.5b. (MATLAB model). It is seen that with almost 20 modes on each waveguide, the S parameter is converging.

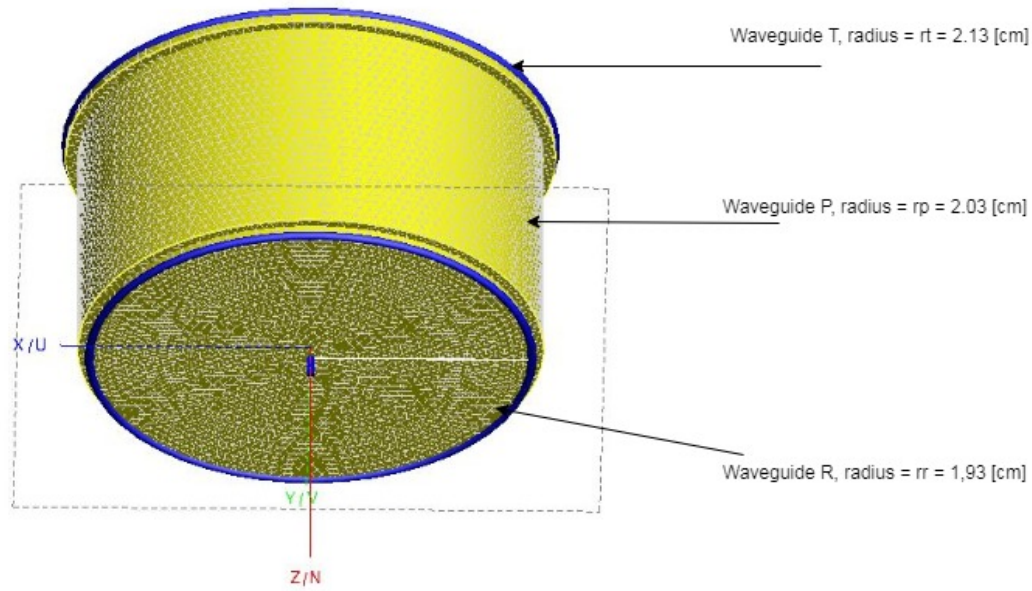
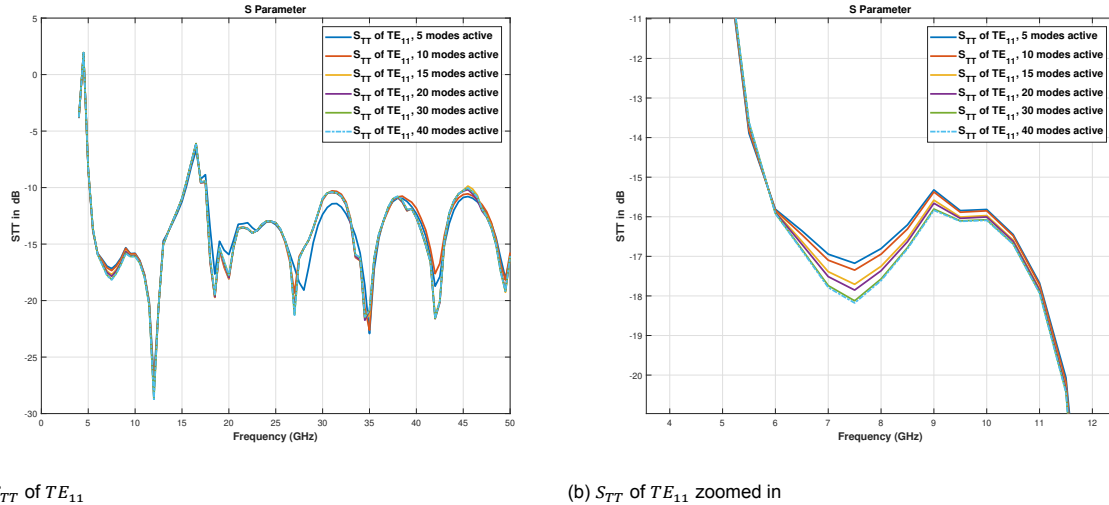


Figure 4.4: 3 waveguides geometry used for simulation.

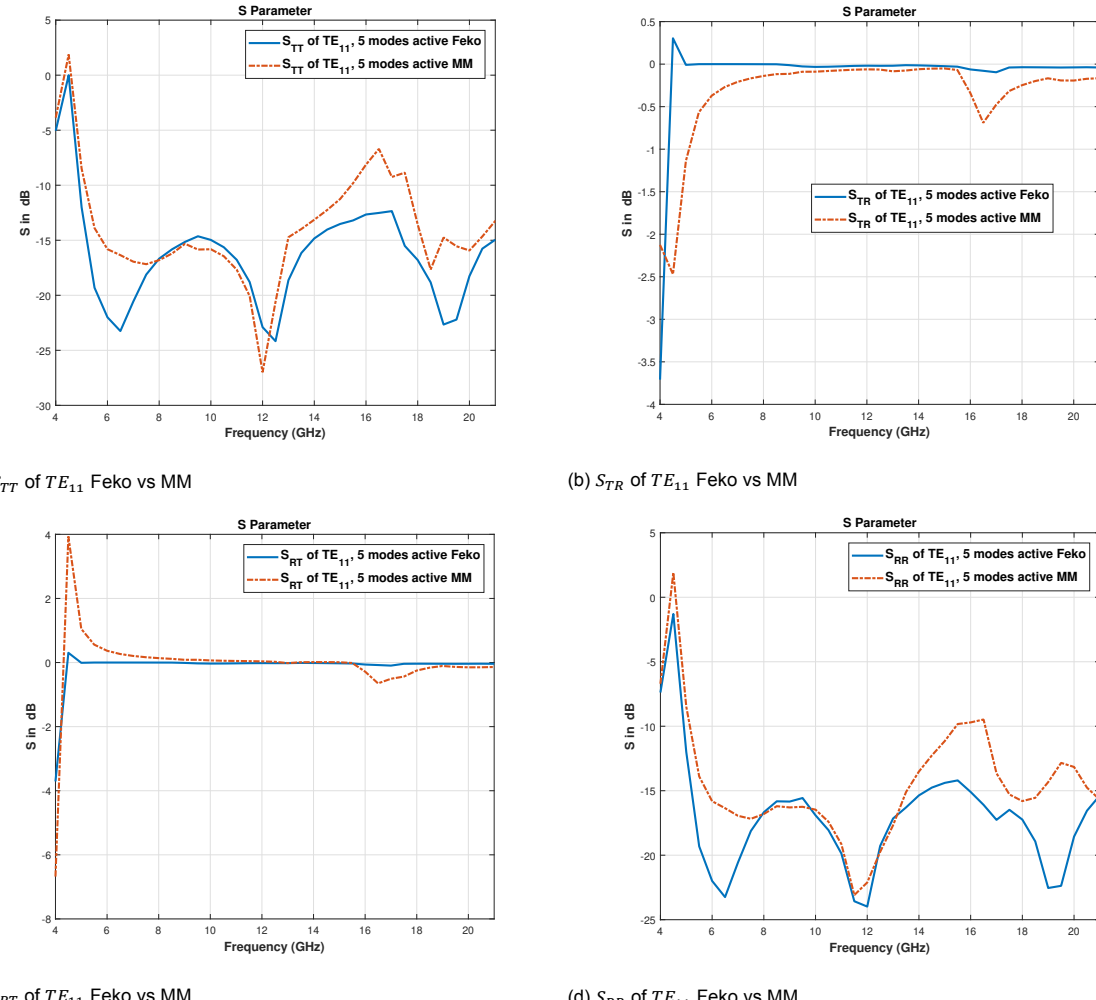
#### 4.1.2. Feko simulation and comparison

The structure in figure 4.4 is simulated on Feko and the results are shown in figure 4.6 when 5 modes are active on each waveguide. It is compared with the solution given with Mode Matching Technique. As we didn't see good convergence with 5 modes on every side, here also we can see some differences at the positions and levels of maxima and minima. However, the trend looks the same. Simulating more modes on Feko was computationally expensive. Examples with more modes will be given further.



(a)  $S_{TT}$  of  $TE_{11}$  (b)  $S_{TT}$  of  $TE_{11}$  zoomed in

Figure 4.5:  $S_{TT}$  of  $TE_{11}$  mode using MM Technique with 3 circular cross-section waveguide.



(a)  $S_{TT}$  of  $TE_{11}$  Feko vs MM (b)  $S_{TR}$  of  $TE_{11}$  Feko vs MM

(c)  $S_{RT}$  of  $TE_{11}$  Feko vs MM (d)  $S_{RR}$  of  $TE_{11}$  Feko vs MM

Figure 4.6: S parameters for  $TE_{11}$  mode - Feko vs MM. 5 modes active on each waveguide



# Bibliography

- [1] Constantine A. Balanis. *Advanced engineering electromagnetics*. J. Wiley Sons, 2012.
- [2] Frank Bowman. *Introduction to Bessel functions*. Dover, 2018.
- [3] D. J. Hoppe. Generalized scattering matrix technique. *The Telecommunications and Data Acquisition Report*; p. p 89-96, 1988.
- [4] Agostino Monorchio, Raj Mittra, and Giuliano Manara. Modal analysis applied to circular, rectangular, and coaxial waveguides. *Encyclopedia of RF and Microwave Engineering*, 2005. doi: 10.1002/0471654507.em145.
- [5] Jorge A. Ruiz-Cruz, Jose R. Montejano-Garai, and Jesus M. Rebollar. Computer aided design of waveguide devices by mode-matching methods. In Vitaliy Zhurbenko, editor, *Passive Microwave Components and Antennas*, chapter 6. IntechOpen, Rijeka, 2010. doi: 10.5772/9403. URL <https://doi.org/10.5772/9403>.
- [6] Tak Sum Chu and T. Itoh. Generalized scattering matrix method for analysis of cascaded and offset microstrip step discontinuities. *IEEE Transactions on Microwave Theory and Techniques*, 34(2):280–284, Feb 1986. ISSN 1557-9670. doi: 10.1109/TMTT.1986.1133323.
- [7] Eric W. Weisstein. "lommel's integrals." from mathworld—a wolfram web resource. URL <http://mathworld.wolfram.com/LommelsIntegrals.html>.